Volume VI
EMERGING and PERIPHERAL TECHNOLOGIES
H.R. Warner Jr., Editor

PETROLEUM ENGINEERING HANDBOOK
Larry W. Lake, Editor-in-Chief

SOCIETY OF PETROLEUM ENGINEERS

Petroleum Engineering Handbook

Larry W. Lake, Editor-in-Chief
U. of Texas at Austin

Volume VI

Emerging and Peripheral Technologies

H.R. Warner Jr., Editor
Consultant

Society of Petroleum Engineers

Volume VI
EMERGING and PERIPHERAL TECHNOLOGIES
H.R. Warner Jr., Editor

PETROLEUM ENGINEERING HANDBOOK
Larry W. Lake, Editor-in-Chief

Manufactured in the United States of America.

ISBN 978-1-55563-122-2 (print)
ISBN 978-1-55563-123-9 (CD)
ISBN 978-1-55563-133-8 (print and CD)
ISBN 978-1-55563-126-0 (Complete 7-Vol. Set, print)
ISBN 978-1-55563-127-7 (Complete 7-Vol. Set, CD)
ISBN 978-1-55563-135-2 (Complete 7-Vol. Set, print and CD)

07 08 09 10 11 12 13 14 / 9 8 7 6 5 4 3 2 1

Society of Petroleum Engineers
222 Palisades Creek Drive
Richardson, TX 75080-2040 USA

http://store.spe.org/
service@spe.org
1.972.952.9393

SOCIETY OF PETROLEUM ENGINEERS

Chapter 12
Electromagnetic Heating of Oil

Roberto C. Callarotti, Inst. Venezolano de Investigaciones Científicas (IVIC)

12.1 Introduction

The electromagnetic heating of oil wells and reservoirs refers to thermal processes for the improved production of oil from underground reservoirs. The source of the heat, generated either in the wells or in the volume of the reservoir, is the electrical energy supplied from the surface. This energy is then transmitted to the reservoir either by cables or through metal structures that reach the reservoir. The main effect, because of the electrical heating systems used in practice in enhanced oil recovery, has been the reduction of the viscosity of heavy and extra heavy crudes and bitumens, with the corresponding increase in production. This chapter mainly considers those systems (and the models that describe their effects) that have been used for the electromagnetic heating in the production of extra heavy petroleum and bitumen. The importance of these hydrocarbons is because of the size of the heavy oil reserves in Canada, Venezuela, countries of the former U.S.S.R., the U.S.A., and China.[1–3]

As shown in **Fig. 12.1**, $Q(t)$, the time-dependent rate of production of a given reservoir with either horizontal or vertical wells, depends on the flow of oil through the reservoir and through the producing wells. In the reservoir, the flow is conditioned by a temperature-dependent viscosity, $\mu(T)$, porosity, permeability, and compressibility (ϕ, k, and c). To a first approximation, the last three parameters are unchanged by the heating. In the wells, the flow is conditioned by the geometry of the wells (radius, depth, and length, in the case of horizontal wells) and again by the oil viscosity.

The heating effect in the porous media of the reservoirs is simply represented by Darcy's law with a temperature-dependent viscosity, $\mu(T)$.

$$\vec{V} \equiv -\frac{k}{\mu(T)}\vec{\nabla}P\left(\vec{r}, t\right), \quad \text{(12.1)}$$

where

$\vec{V}$ = fluid velocity,

k = effective permeability,

and

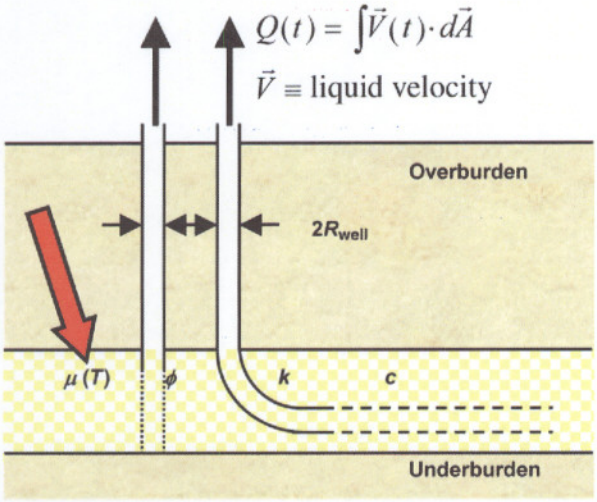

Fig. 12.1—Typical vertical and horizontal well arrangements. Heating strongly affects the viscosity of the oil in the reservoir porous media and in the wells.

$P\left(\vec{r}, t\right)$ = the space- and time-dependent pressure.

The effect of the heating in a well (along the z direction), is represented by a temperature-dependent viscosity used in the Hagen-Poiseville law.

$$V_z \equiv -\frac{(R_{well})^2}{8\mu(T)} \frac{\partial P(z, t)}{\partial z}, \quad \text{..... (12.2)}$$

where R_{well} = the radius of the well.

The viscosity, μ, is related to the kinematic viscosity, ν, by the relation

$$\mu = \rho\nu, \quad \text{..... (12.3)}$$

where ρ is the density of the hydrocarbon. The strong temperature dependence of the viscosity ν (for values of kinematic viscosities ν above 2 mm²/s) is given by the law shown in Eq. 12.4.[4]

$$\log[\log(\nu + 0.7)] = A_1 - A_2 \log(T), \quad \text{..... (12.4)}$$

where A_1 and A_2 are characteristic constants for each liquid hydrocarbon (with no dissolved gases), and T is the absolute temperature. As shown schematically in **Fig. 12.2**, in the range of reservoir temperatures (40 to 60°C), a temperature increase of a few degrees can reduce the viscosity significantly with the corresponding increase in production. For 9.9°API oil, a temperature increase from 30 to 40°C reduces the viscosity by 67%, an increase from 40 to 50°C causes a 62% reduction, and an increase from 50 to 60°C reduces the viscosity by 57%. The corresponding production increases depend on the temperature spatial distribution throughout the reservoir and in the well system.

As in many other applications of electrical heating and in the case of well and reservoir heating, there is a wide range of available frequencies in the electrical spectrum, which can be used in diverse heating schemes. At the low-frequency (LF) end, energy is supplied directly from the 60 Hz distribution grid.[5] Induction heating requires higher frequencies in the radio frequency (RF) range of 10^3 to 10^5 Hz, while heating is also possible at frequencies in the

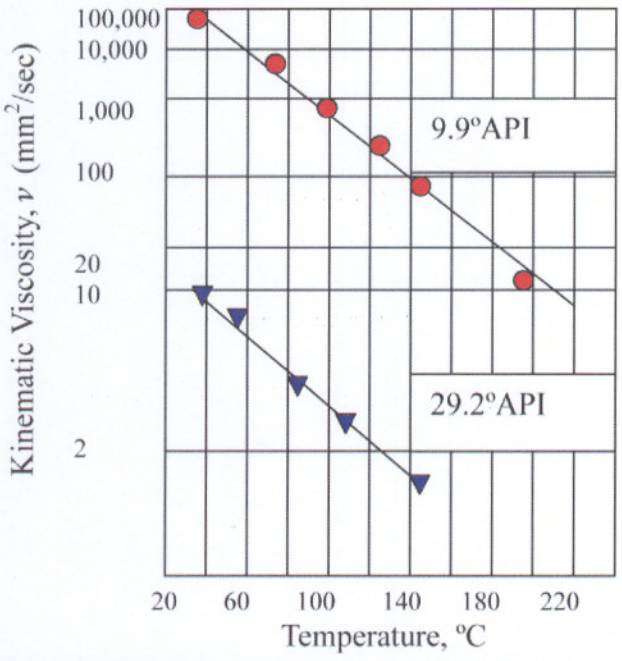

Fig. 12.2—Temperature dependence of the kinetic viscosity of oil for different densities.

microwave (MW) range (MW 10^9 to 3×10^{10} Hz).[6] So far, most of the enhanced oil recovery (EOR) heating schemes used successfully in the oil industry have been in the low-frequency range. Microwave heating has been widely used industrially in the past, but its application to reservoir heating is not widespread, although it has been receiving more attention lately.[7–9]

The analysis of low-frequency heating up to radio frequencies, can be carried out through a circuital approach based on the application of Kirchhoff's laws: the voltage law (KVL) for voltages around a loop, and the current law (KCL) for currents into a node. In this range of frequencies, the process is commonly defined as electrical heating and the parameters used are voltage, current, resistance, capacitance, and inductance. The analysis of microwave heating processes requires the full description provided by electromagnetic theory, as described by Maxwell's field equations in terms of electric and magnetic field vectors, $\vec{E}$,$\vec{H}$, vector current density, $\vec{J}$, with material properties represented by permittivity, ε, permeability, μ_M, and conductivity, σ. In this range, the process is correctly defined as electromagnetic heating. The case of induction heating can be described through a mixed approach.

12.1.1 Concentrated Heating Scheme: Resistive LF and Inductive RF. In the case of vertical wells, **Figs. 12.3a and 12.3b** illustrate the possible concentrated heating schemes that have been proposed and used in practice. In this concentrated case, a heating unit is located in the well at the depth of the producing zone. The heating is generated locally over the heater volume and then transferred to the system. Heat flow is conductive and convective in the reservoir and well volumes, and conductive in the rest of the system. Radiative heat transfer is generally not considered, in view of the low range of temperatures obtained.

In the case of resistive concentrated heating, the heating unit consists of one or more resistances (in Fig. 12.3a, we show a Wye-connected three-phase arrangement) connected by a set of metallic conductors to a surface power supply (which in the simplest of cases is a 60 Hz source connected to the power grid). As shown in Fig. 12.3b, in the case of inductive concen-

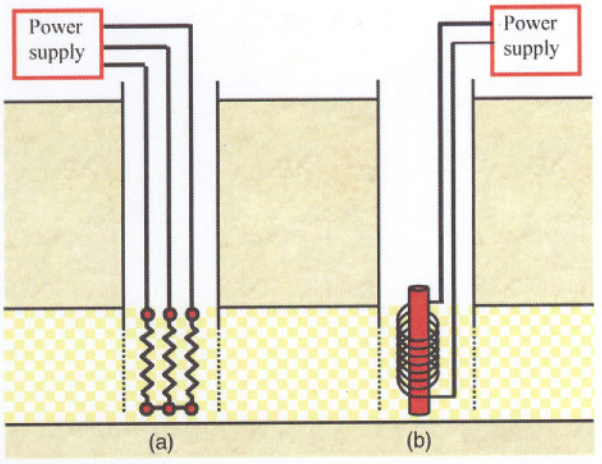

Fig. 12.3—Typical schemes for concentrated heating: (a) three-phase resistive heating and (b) inductive heating with a coil around a metallic core.

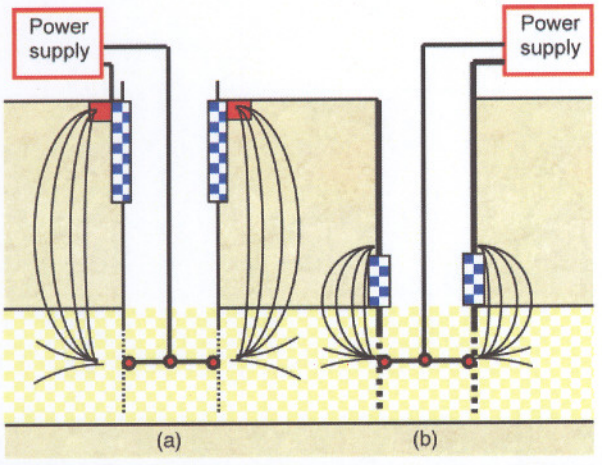

Fig. 12.4—Typical schemes for distributed resistive heating: (a) a less-efficient scheme, as most of the current flow is outside the reservoir section; (b) using the casing as a terminal improves the scheme by localizing more of the electrical losses (heating) in the reservoir area. The dotted regions represent the electrically isolated sections of casing.

trated heating, the heating unit consists of a coil wound around a core of metal. The coil is connected by a set of metallic conductors to a surface power unit, which can operate at frequencies up to several kHz, deriving its primary power from the 60-Hz power grid.

12.1.2 Distributed Heating Scheme: Resistive LF. The case of distributed resistive heating is shown in Fig. 12.4. In this case, an external power supply (generally fed from the 60-Hz power grid) generating low-frequency currents and voltages is connected by cable to a pressure device in contact with the perforated section of the production casing, while the other terminal is either connected to ground at the surface (a) or at some lower level (b).

In either case, electrical current flows through the overburden, reservoir and underburden, and in each volume element of material, it dissipates electrical power in accordance with the value of the resistance and capacitance per unit volume of the different media. Sections of

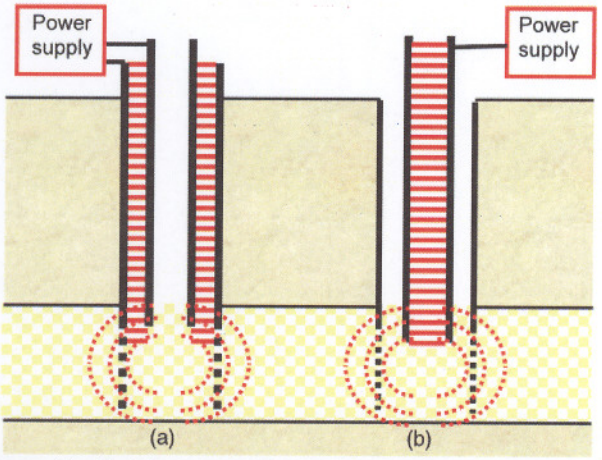

Fig. 12.5—Typical schemes for high-frequency electromagnetic power transfer from the surface to the reservoir (the hatched area indicates the region where electromagnetic power is located). In (a), the energy is transmitted in the space between the casing and the production tubing, while in (b), the energy propagates along the waveguide provided by the production tubing.

insulated tubing are required to direct most of the current flow into the reservoir, thus, keeping the generated power within the reservoir volume. This scheme has been described in the literature as electromagnetic heating, although this term should be strictly applied to those cases in which the frequencies used are much higher than 60 Hz.

12.1.3 Distributed Microwave Heating Scheme. As described later in this chapter, high- frequency electromagnetic energy can be transferred from power supplies situated at the surface to the reservoir region by the structures shown on Fig. 12.5. In the first arrangement (a), energy is transmitted in the annular space between the casing and the production tubing in the form of transverse electromagnetic (TEM) waves. In the second case (b), energy is transmitted along the production tubing in the form of transverse electric (TE) or transverse magnetic (TM) modes. The schemes shown do not require cables to be connected to the source at the surface, which implies a great reduction in installation complexities. Coaxial cables can of course also be used for the transmission of TEM waves from the surface to the reservoir. In all cases some sort of radiating element must be situated in the well at reservoir depth, in order to transfer electromagnetic energy to the reservoir.

12.2 Historical Perspective

12.2.1 Low-Frequency Resistive Heaters. Downhole concentrated electrical heaters have been used for many years. Their early applications, prior to 1969 both in the former U.S.S.R. and the United States, have been reviewed by Farouq Ali who described more that 70 wells stimulated electrically in the U.S.S.R. and some 60 wells in California.[10] In a second publication, Farouq Ali discussed the first patents issued in the U.S.S.R. (in 1934) and in the U.S.A. (in Fig. 12.2.1—1951).[11] The structure of the heaters, shown in Fig. 12.6, has not changed significantly in time.*[,12]

The heating elements consist of iron-nickel-chromium or nickel-chromium alloy wires wound on high-thermal-conductivity materials with low electrical losses, enclosed in metallic cylindrical sheaths. The resistive wires could also be surrounded by compacted magnesium ox-

* Personal communication with J. Rau, Petrotherm, Tía Juana, Venezuela (1997).

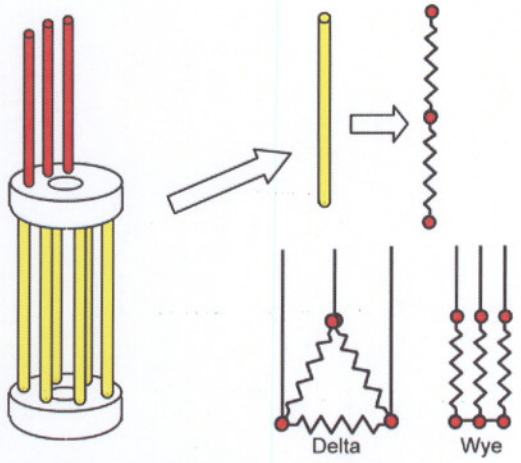

Fig. 12.6—The structure of concentrated resistive downhole heaters fed by three-phase 60 Hz electrical power. The heating elements can be connected in Delta or Wye structures.

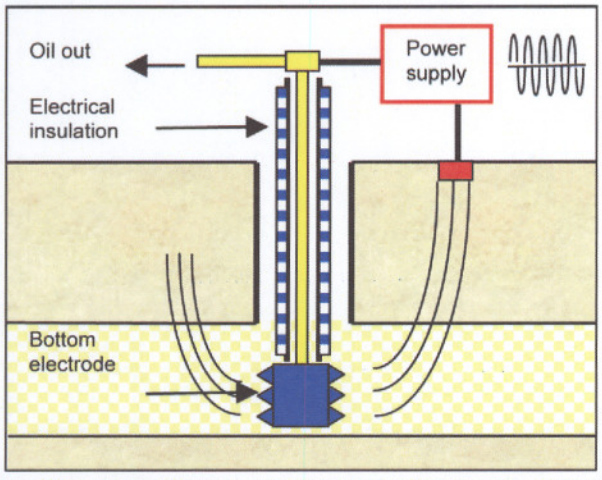

Fig. 12.7—The structure of the electrothermic process where single-phase sinusoidal, 60 Hz, 480 volt power is fed to a downhole contactor through an insulated production pipe.

ide powder.[13,14] According to Orfeil, the use of the heating elements is restricted to surface power densities lower than 2 watts/cm^2 because of maximum temperature limitations.[5]

12.2.2 High Frequency to Microwave-Distributed Heating. In 1976, Abernethy first described microwave-distributed heating (refer to Fig. 12.5), including a complete model of the proposed process (discussed later in this chapter).[15]

12.2.3 Distributed Low-Frequency Heating. In 1979, Gill reported the first low-frequency single-phase distributed heating system applied in oil fields in Texas, Utah, and Mexico.[16] It is described as an electrothermic system for EOR and uses the structure shown in **Fig. 12.7**, with voltage excitations of 480 volts at 60 Hz.

Vinsome *et al.* described recent versions of commercially available distributed heating systems.[17] The power-supply current flows through "tubing, cables or a combination of both." A

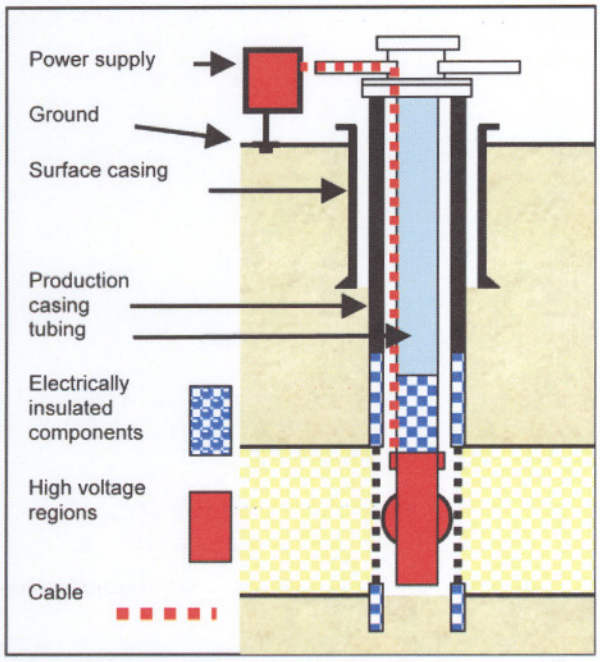

Fig. 12.8—Scheme for distributed low-frequency resistive heating. The production pipe remains at ground potential.

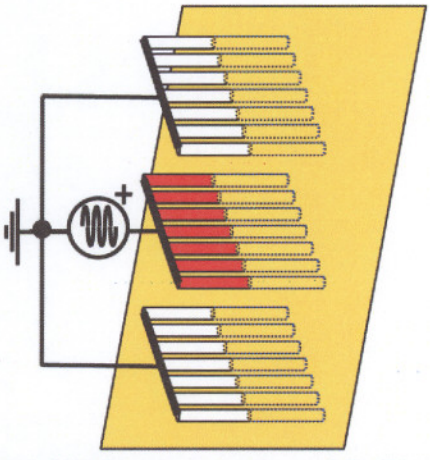

Fig. 12.9—Scheme for concentrated high-frequency heating (13.56 MHz). The inserted electrode arrays play the role of capacitor plates, restricting most of the fields to the space between them.

possible system, in which the power supply is connected by cable to the lower section of the production tubing that is in electrical contact with the reservoir through the perforated metallic casing, is shown in Fig. 12.8.

12.2.4 High-Frequency Concentrated Heating. In 1979, Bridges *et al.* wrote a conceptual paper on the possible use of radio frequency (10 KHz to 10 MHz) power for the heating of Utah tar sands, applied through a set of metallic electrodes inserted into the surface reservoir much like a set of capacitors.[18] The scheme proposed is shown in Fig. 12.9.

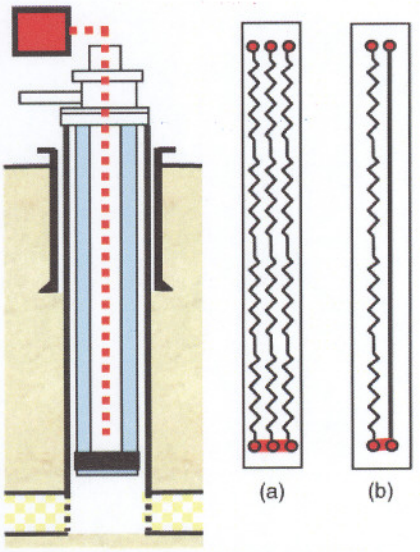

Fig. 12.10—Possible arrangements for distributed resistance heating of wells with electrical cables inside hollow pump rods: (a) three-phase, (b) one-phase.

Carlson *et al.* and Sresty *et al.* reported the results of the field tests of high-frequency (2.2875 MHz and 13.56 MHz) heating at 20 to 40 kW power levels in Utah.[19,20] The first successful test used an implanted horizontal electrode array, which covered a 1 m^3 volume of material. A second test, covering a volume of 25 m^3 and heated by a set of vertical electrodes, had to be stopped because of the subsidence of the tar sand mass but was later completed when the roof support was improved.

12.2.5 Low-Frequency Distributed Resistive Heating Along the Well. Electrical strip heaters (available in continuous lengths between 1,000 and 3,500 ft) situated along the production well pipe have been used in the reduction of waxy deposits for several years. Lately, the use of electrical heaters has been applied to the reduction of hydrates deposits in pipelines.[21]

The 1995 published field results by Cheng *et al.* show several wells thermally excited by distributed resistive heating that was provided for by cables inside hollow pump rods.[22] The arrangement, shown in Fig. 12.10, is representative of a distributed resistive heating system for wells.

12.2.6 Distributed LF Resistive Heating in Vertical/Horizontal Wells. McGee and Vermeulen described the application of distributed heating in horizontal/vertical well Fig. 12.2.6—combinations.[23] The structure, proposed for their system, is essentially that which is shown in Fig. 12.11.

12.2.7 Process Modeling: Theoretical and Physical. In 1957, Schild carried out the first complete steady-state modeling of concentrated heaters and also reported on earlier uses of these heaters.[24] Abernethy first proposed a theoretical scheme examining the possibility that microwave frequency waves could propagate in a reservoir.[15] He compared the steady-state temperature distribution, produced by this high-frequency distributed heating scheme, with the temperature distribution produced by concentrated heating. No comparison was presented for the transient production rate of the two methods.

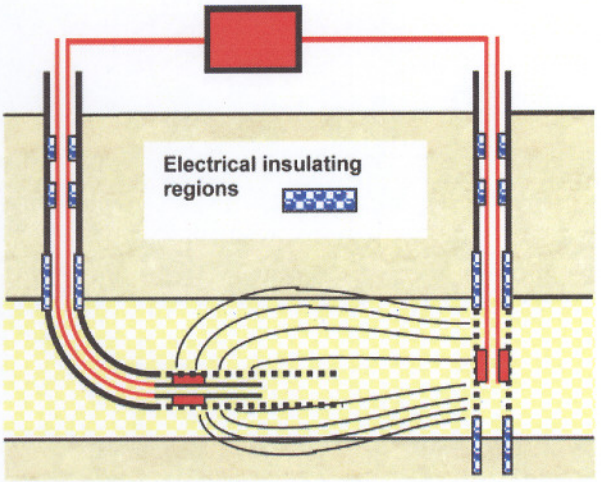

Fig. 12.11—Distributed heating scheme proposed by McGee and Vermeulen.[23]

A numerical analysis for a distributed system based on a Canadian patent was published in 1978 by Todd and Howell.[25] Convection effects were not considered and the distributed electrical power was determined by a resistive circuital network.

Calculations by Newbold and Perkins determined the possible losses incurred in the electrical transmission of low-frequency power (60 Hz to 2,400 Hz) from the surface to the reservoir production level.[26] Both Eddy-current losses and magnetic losses were considered for transmission through wire cables or through the tubing system.

Harvey *et al.* discussed a laboratory simulation for simultaneous waterflooding and distributed resistive heating, and Harvey and Arnold modeled the concurrent radial flow of low-frequency electrical currents and injected water (heat conduction to overburden and underburden is disregarded).[27,28]

Vermeulen and Chute described physical models for distributed conduction heating and for inductive localized heating,[27–29] and McPherson *et al.*[30] modeled the steady-state excitation of Athabasca bitumen at varying frequencies from 60 Hz to 250 kHz using transmission line theory to improve the model of the metallic electrodes. Bridges *et al.* discussed the electromagnetic stimulation of heavy oil wells.[31,32]

Killough and Gonzalez presented a numerical model of well-to-well distributed conductive heating, which is compared with previous experimental results of El-Feky.[33,34] They compare DC power excitation and three phase excitation, but no capacitive (or permittivity) characteristics of the system were given, and no frequency effects were reported.

In 1986, Hiebert *et al.* presented a numerical two-dimensional (2D) simulator for low-frequency (60-Hz) distributed heating but ignored convection heat flow.[35] They included a list of patents related to this heating scheme.

Casey and Bansai calculated the near field, produced by a dipole antenna.[36] And in 1989, Callarotti described the frequency limitations of resistive-capacitive (R-C) circuits.[37] Pizarro and Trevisan presented a model, applied to a 1987 distributed heating test, that was carried out in the Rio Panon field in Brazil.[38] Their model did not include convection terms or heat losses to regions outside the producing zone but considered both oil and water phases.

Fanchi, in 1990, examined the propagation of cylindrical transverse electromagnetic waves into the reservoir, showing the validity of the model used by Abernethy if the reservoir is far away from the radiating source.[15,39] Also, in the same year, Baylor *et al.* discussed the reservoir steady-state response to low-frequency resistive distributed heating at the SPE Annual

Technical Conference and Exhibition.[40] Islam *et al.* discussed distributed low-frequency heating of horizontal wells at a conference in 1991.[45] And in the same year, at the UNITAR conference, electrical heating was discussed, including microwave heating and high-frequency Fig. 12.2.7—modeling.[42–46]

In 1992, Callarotti and Di Lorenzo used R-C circuital modeling in core tomography, while Sumbar *et al.* presented a numerical model for distributed low-frequency heating, which correctly includes the convective heat transfer but only considers one phase of fluid (incompressible oil) driven by a pressure source at the reservoir outer radius.[47,48] One year later, Dolande and Datta provided analytical solutions to one-dimensional (1D) conductive heat transfer problems in the presence of radiated power exponentially decreasing in space.[49]

In the mid-1990s, Callarotti published the application of circuital modeling to the transient solution of fluid flow in porous media, as well as a new numerical method that avoids time iterations.[50,51] Later, Callarotti and Mendoza compared the transient and steady-state response of concentrated vs. distributed heating for different fixed production rates (the fluid flow equation was not solved).[52]

Soliman presented an approximate numerical model for the electrical heating of reservoir at power levels in which the water is vaporized.[53] Also in 1999, Hu *et al.* presented the results of a physical model with high-frequency heating (5 to 20 MHz).[54]

12.2.8 Measurements. The conductivity of medium heavy oil, including its temperature dependence, was measured by Kendall in 1978.[55] Snow and Bridges, from the Illinois Inst. of Technology, reported laboratory experiments in which radio-frequency power (in the range of 100 to 300 KHz) was applied to oil shales, and the results were compared with pyrolysis experiments.[56,57]

Later, in the early 1980s, Butts *et al.* measured microwave heating (at 2,450 MHz) of New Brunswick oil shales.[58] Briggs *et al.* measured the response of New Brunswick oil shales at high frequencies in three bands: 10 to 1,000 MHz, 2 to 4 GHz, and 8 to 12 GHz, reporting a permittivity of $\varepsilon = \varepsilon_0\ (3.5 - j0.2)$ at 915 MHz, and Vermeulen and Chute measured samples from the Athabasca deposits in a frequency range from 50 Hz to 1 GHz.[29,59]

The effect of interfacial polarization phenomena, in which diffusion current and space charge are considered at the solid/liquid interphases, was discussed by Sen and Chew.[60] They included a discussion of the anomalously high values of the dielectric constants of wet rocks (up to 1,000) that were previously discussed by Poley *et al.*[61] The situation occurring in these heterogeneous solid/liquid systems is certainly complex—a well-known fact in impedance spectroscopy electrochemical measurements.

The case of oil by itself, out of the reservoir, is much simpler. It is characterized by a very small conductivity: $\sigma = 2.5 \times 10^{-8}$ siemens/m for medium heavy oil with 0.9 gravity.[55] Dielectric constant measurements show no surprises over the frequency range from 100 Hz to 3 GHz, with a measured permittivity of $\varepsilon = \varepsilon_0\ (2.3 - j0.011)$ at high frequencies.*

12.2.9 Reviews and General References. In 1987, Prats published an updated version of his 1982 monograph on thermal methods, which includes a review of electrical heating methods.[62] Also, in the same year, Vermeulen and Chute suggested a nomenclature to be used for electromagnetic heating processes in accordance to different approximations in Maxwell's equations.[63] Chute and Vermeulen reviewed actual and potential applications of electrical heating for oil production and included complete references on the subject.[64] Duncan reviewed electrical heating schemes and included well designs and completion practices.[65]

* Personal communication with W.B. Westphal, formerly with the MIT Laboratory for Insulation Research, Cambridge, Massachusetts (1994).

Selyakov and Kadet published a textbook on percolation processes in porous media, in which the microscopic descriptions of alternating currents, acoustic waves, and dissipation effects are discussed.[66] Other textbooks, edited by Kraszewski and by Kinston and Haswell, represent excellent references on the interaction of electromagnetic energy with water-containing and other materials.[67,68]

12.3 Electrical Engineering Considerations

In most practical situations we are concerned with field that vary periodically in time (the sinusoidal steady state generally). In these cases the electrical phenomena are properly described by Maxwell equations in terms of complex vector field intensities of electric and magnetic fields ($\vec{E}$ and $\vec{H}$); complex vector field electric, magnetic, and current densities ($\vec{D}, \vec{B}, \vec{J}$); complex charge concentrations (ρ_c); and complex material parameters: conductivity, permittivity, and permeability (σ, ε, μ_M). For the case of sinusoidal excitations [exp ($j\omega t$)] and in the absence of diffusion currents, these equations are listed next.

$$\vec{\nabla} \times \vec{E} = -j\omega \vec{B} \,. \qquad (12.5)$$

$$\vec{\nabla} \times \vec{H} = \vec{J} + j\omega \vec{D} \,. \qquad (12.6)$$

$$\vec{\nabla} \cdot \vec{D} = \rho_c \,. \qquad (12.7)$$

$$\vec{\nabla} \cdot \vec{B} = 0 \,. \qquad (12.8)$$

$$\vec{D} = \varepsilon(\omega)\vec{E} = \left[\varepsilon'(\omega) - j\varepsilon''(\omega)\right]\vec{E} \,. \qquad (12.9)$$

$$\vec{B} = \mu_M(\omega)\vec{H} = \left[\mu'(\omega) - j\mu''(\omega)\right]\vec{H} \,. \qquad (12.10)$$

$$\vec{J} = \sigma(\omega)\vec{E} = \left[\sigma'(\omega) - j\sigma''(\omega)\right]\vec{E} \,. \qquad (12.11)$$

As indicated, the material parameters are frequency-dependent complex numbers. Of course, $\omega = 2\,\pi\, f$, where the frequency, f is given in cycles per second (Hz).

The physical fields vectors correspond to the real part of the complex field vector times [exp ($j\omega t$)]. For example, the physical electric field vector is given by Real[$\vec{E}$ exp ($j\omega t$)].

The power radiated per unit area is given by the complex Poynting vector, $\vec{S}$, defined as

$$\vec{S} \equiv \frac{1}{2}\vec{E} \times \vec{H}^* \,, \qquad (12.12)$$

where * indicates complex conjugate.

For the volume, V, enclosed by a surface, A, indicated in Fig. 12.12, the volume integral of the divergence of the complex Poynting vector, $\vec{S}$, yields

$$-\int \vec{S} \cdot d\vec{A} = \frac{j\omega}{2}\int\left(\mu'\vec{H}\cdot\vec{H}^* - \varepsilon'\vec{E}\cdot\vec{E}^*\right)dV + \frac{j}{2}\int\sigma''\left(\vec{E}\cdot\vec{E}^*\right)dV$$
$$+\frac{1}{2}\int\sigma'(\omega)\left(\vec{E}\cdot\vec{E}^*\right)dV + \frac{\omega}{2}\int\left(\mu''\vec{H}\cdot\vec{H}^* + \varepsilon''\vec{E}\cdot\vec{E}^*\right)dV \,. \qquad (12.13)$$

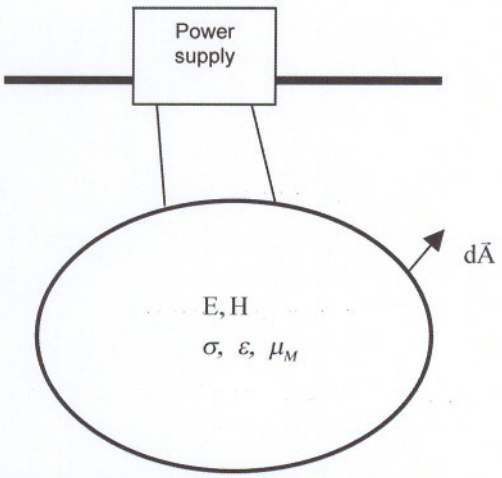

Fig. 12.12—A given volume, *V*, enclosed by a surface, *A*, excited from a surface power supply.

This equation represents a balance of power for the volume shown.[69] The left-hand side represents the total power entering the volume through its surface. The first two right hand terms represent the power stored in the volume, while the last two terms represent the power dissipated in the volume. This dissipated power depends on the real part of the conductivity and the magnitude of the local electric field (third term), the imaginary parts of the magnetic permeability and electrical permittivity of the material enclosed in the volume, and the magnitudes of the magnetic and electric fields (fourth term). If the permeability and permittivity are real, the only power loss is owing to the real part of the conductivity and the magnitude of the local electric field.

Thus, the power radiated into the volume is equal to the rate of increase of the stored energy in the volume, plus the power dissipated (because of the real part of the conductivity and the imaginary parts of permittivity and permeability, and the magnitudes of the corresponding fields). Thus, the real power dissipated per unit volume, P_{PUV}, is given by

$$P_{PUV} = \frac{1}{2}\left\{\left[\sigma'(\omega) + \omega\varepsilon''(\omega)\right]\left(\vec{E}\cdot\vec{E}^{*}\right) + \omega\mu''(\omega)\left(\vec{H}\cdot\vec{H}^{*}\right)\right\}. \quad \text{..... (12.14)}$$

This is the term that enters the differential equation for the heat distribution. Among other factors, the power depends on the magnitudes of the local electric and magnetic fields. In those cases where the electrical power is generated at the surface of the earth, these magnitudes will depend on the transmission power losses from the surface to the reservoir.

The vector wave equation for exp (*jωt*) excitation, space independent (σ, ε, μ_M), no diffusion currents, and ρ_C=0. Proper knowledge of the issues involved in the transmission and dissipation of electrical power for the heating of wells and reservoirs can only be obtained by examining the solution of the vector wave equations. The wave equations are derived from Maxwell's equations.[70–72]

$$\vec{\nabla}^2\vec{E} + \gamma^2\vec{E} = 0;\ \vec{\nabla}^2\vec{H} + \gamma^2\vec{H} = 0\,. \quad \text{..... (12.15)}$$

The propagation constant, γ, is defined as

$$\gamma^2 \equiv \left[\omega^2 \mu_M(\omega)\varepsilon(\omega) - j\omega\sigma(\omega)\mu_M(\omega)\right] . \quad (12.16)$$

For their relevance to the heating oil problem, we will consider solutions in rectangular Cartesian coordinates x, y, z and in cylindrical coordinates, r,ϕ,z. We will first discuss the rectangular Cartesian coordinate case.

Rectangular coordinates: plane wave propagation in the z direction (an assumed direction of power or energy flow). Under these conditions, we have:

$$\frac{\partial}{\partial x} = 0; \frac{\partial}{\partial y} = 0, \quad (12.17)$$

$$\vec{H} = H(z)\,\vec{i}_y, \quad (12.18)$$

$$\text{and } \vec{E} = E(z)\,\vec{i}_x . \quad (12.19)$$

Then, the wave equations have these solutions:

$$E(z) = \left\{A_+ \exp(-j\gamma z) + A_- \exp(+j\gamma z)\right\} \exp(j\omega t) . \quad (12.20)$$

$$H(z) = \frac{\gamma}{\mu_M \varepsilon}\left[A_+ \exp(-j\gamma z) - A_- \exp(+j\gamma z)\right] \exp(j\omega t) . \quad (12.21)$$

A_+ and A_- are integration constants defined by the boundary conditions of the problem. Thus, the solutions for propagation in free space along the positive z-axis ($\sigma = 0$, $\varepsilon = \varepsilon_0 = 8.854 \times 10^{-12}$ farads/m, the permittivity of vacuum, $\mu_M = \mu_0 = 4\pi \times 10^{-7}$ henrys/m, the permeability of vacuum) are

$$E^+_{FS}(z) = A_+ \exp\left(j\omega t - j\gamma_0 z\right) \equiv A_+ \exp\left[-j\gamma_0\left(z - V_0 t\right)\right] . \quad (12.22)$$

These equations represent waves propagating in the $+z$ direction with velocity, V_0 (the speed of light in vacuum), a wavelength, λ_0, and a wave impedance, Z_0.

$$H^+_{FS}(z) \equiv \frac{1}{Z_0} A_+ \exp\left(j\omega t - j\gamma_0 z\right) . \quad (12.23)$$

$$\gamma_0 \equiv \omega\sqrt{\left(\varepsilon_0 \mu_0\right)} \equiv \frac{2\pi}{\lambda_0} . \quad (12.24)$$

$$V_0 \equiv \frac{1}{\sqrt{\left(\varepsilon_0 \mu_0\right)}} = 3.0 \times 10^8 \text{ms}^{-1} . \quad (12.25)$$

$$\lambda_0 \equiv \frac{2\pi}{\omega\sqrt{\left(\varepsilon_0 \mu_0\right)}} = \frac{V_0}{f} . \quad (12.26)$$

TABLE 12.1—FREQUENCY-WAVELENGTH RELATIONS FOR FREE SPACE

Band Name	Frequency Range	Free Space Wavelength, m
Cosmic rays	Greater that 10^{+20}	Less than 10^{-12}
Gamma rays	$3\times10^{+20}$ to $3\times10^{+19}$	10^{-12} to 10^{-11}
X-rays	$3\times10^{+19}$ to $3\times10^{+18}$	10^{-11} to 10^{-10}
Ultraviolet	$3\times10^{+18}$ to $7\times10^{+14}$	10^{-10} to 4.3×10^{-7}
Visible light	$7\times10^{+14}$ to $4\times10^{+14}$	4.3×10^{-7} to 7.5×10^{-7}
Infrared	$4\times10^{+14}$ to 300 GHz	7.5×10^{-7} to 10^{-3}
EHF (extra high)	300 GHz to 30 GHz	10^{-3} to 10^{-2}
SHF (super high)	30 GHz to 3 GHz	10^{-2} to 10^{-1}
UHF (ultra high)	3 GHz to 300 MHz	10^{-1} to 1
VHF (very high)	300 MHz to 30 MHz	1 to 10
HF (high)	30 MHz to 3 MHz	10 to 100
MF (middle)	3 MHz to 300 kHz	10^{+2} to 10^{+3}
LF (low)	300 kHz to 30 kHz	10^{+3} to 10^{+4}
VLF (very low)	30 kHz to 3 kHz	10^{+4} to 10^{+5}
ULF (ultra low)	Less than 3 kHz	Greater than 10^{+5}

$$Z_0 \equiv \sqrt{\left(\frac{\mu_0}{\varepsilon_0}\right)} = 377 \text{ ohm} . \quad \text{..... (12.27)}$$

Table 12.1 shows the variety of wavelengths for propagation in free space as a function of frequency, f.

The effect of losses ($\sigma = \sigma' - j\sigma''$, $\varepsilon = \varepsilon' - j\varepsilon''$, $\mu_M = \mu' + j\mu''$) on the solutions makes the propagation constant, γ, become

$$\gamma = \sqrt{\omega(\mu' - j\,\mu'')\left[\omega(\varepsilon' - j\,\varepsilon'') - j(\sigma' - j\sigma'')\right]} \equiv \beta + j\,\alpha,$$
$$\beta \equiv \text{Real}\,(\gamma),\ \alpha \equiv \text{Imag}\,(\gamma), \quad \text{..... (12.28)}$$

where j is the complex unit, and the fields are

$$E^{+}(x) = A_{+} \exp\{j\omega t\} \exp\{-j\beta x\} \exp\{\alpha x\} \quad \text{..... (12.29)}$$

and

$$H^{+}(x) \equiv \frac{\gamma}{\omega\mu_M} A_{+} \exp\{j\omega t\} \exp\{-j\beta x\} \exp\{\alpha x\} . \quad \text{..... (12.30)}$$

If $\alpha < 0$, the amplitude of the wave will decrease as it travels in the $+z$ direction. The real power radiated per unit area (P_{PUA}) is

$$P_{\text{PUA}} = \text{Real}\left[\frac{1}{2}\vec{E} \times \vec{H}^{*}\right] = 0.5\left|A^{+}\right|^{2} \text{Real}\left[\frac{\beta - j\alpha}{\omega\,\mu_M^{*}} \exp(2\alpha x)\right] . \quad \text{..... (12.31)}$$

Cylindrical coordinates: wave propagation in the r direction (an assumed direction of power or energy flow). In this case and for uniform wave propagation in the r direction, we have:

$$\frac{\partial}{\partial \phi} = 0; \frac{\partial}{\partial z} = 0 . \quad (12.32)$$

$$\vec{E} = E(r)\vec{i}_z . \quad (12.33)$$

$$\vec{H} = H(r)\vec{i}_\phi . \quad (12.34)$$

The wave equations become

$$\frac{1}{r}\frac{\partial}{\partial r}\left[r\frac{\partial E(r)}{\partial r}\right] + \gamma^2 E(r) = 0, \quad (12.35)$$

and

$$\frac{1}{r}\frac{\partial}{\partial r}\left[r\frac{\partial H(r)}{\partial r}\right] - \left[\frac{H(r)}{r^2}\right] + \gamma^2 H(r) = 0 . \quad (12.36)$$

Bessel's equations provide solutions for wave propagation in the positive r direction[73] in terms of Hankel functions $H_0^{(2)}$ and $H_1^{(2)}$.[74]

$$E(r) = A_+ H_0^{(2)}(\gamma r) \exp(j\omega t) . \quad (12.37)$$

$$H(r) = \frac{j\gamma}{\omega\mu_M} A_+ H_1^{(2)}(\gamma r) \exp(j\omega t) . \quad (12.38)$$

The nature of the waves propagating in the $+r$ direction is clearly shown observing the limit of the Hankel functions for large arguments ($\gamma r >> 1$).

$$H_0^{(2)}(\gamma r) \Rightarrow H_1^{(2)}(\gamma r) \Rightarrow \sqrt{\frac{2}{\pi\gamma r}} \exp\left\{-j\left[\gamma r - \frac{\pi}{4}\right]\right\} . \quad (12.39)$$

In essence, this is the far-field approximation used by Abernethy.[15] The real power per unit area radiated in the positive r direction is

$$P_{\text{PUA}} = \text{Real}\left(\frac{1}{2}\vec{E} \times \vec{H}^*\right) = 0.5 \left| A_+ \right|^2 \text{Real}\left[\frac{\beta - j\alpha}{\omega \mu_M^*} H_0^{(2)}(\gamma r) H_1^{(2)}(\gamma^* r)\right] . \quad (12.40)$$

12.3.1 Electrode Structures That Allow Transverse Electromagnetic (TEM) Wave Propagation. The metal electrode configurations, shown in **Fig. 12.13**, allow TEM wave propagation for all values of frequency. Both the single-phase (two wires) and three-phase transmission systems shown (normally used for 60 Hz power transmission) have an electromagnetic energy distribution over the cross section of the wires and in the surrounding space. The metal cables simply guide the electromagnetic energy along. In the case of the other structures shown, the fields and the energy are enclosed within the metallic electrodes. The coaxial structure exists naturally in vertical and horizontal wells. It can be used to transfer electromagnetic energy at high frequencies from the surface to the reservoir.

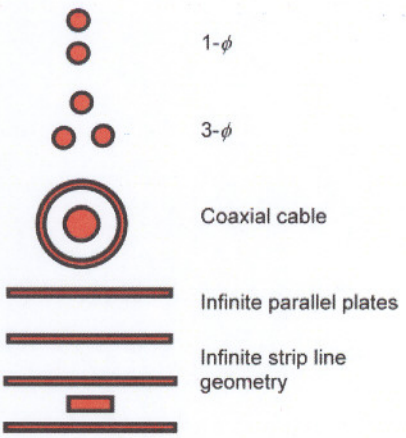

Fig. 12.13—Metallic structures that support TEM waves (no field components along the direction of propagation).

12.3.2 TEM Transmission in Coaxial Lines. The details of the solution for a z-directed coaxial cable (inner radius = r_a, outer radius = r_b) are found in Ref. 75. For an inner electrode material with $\mu_M = \mu_0$ and $\sigma = 0$, the fields and the propagation constant are

$$E_r^+(z) = A_+ \left\{\frac{1}{r}\right\} \exp\{-j\,\gamma\,z\} \exp\{j\omega t\}, \quad \text{(12.41)}$$

$$H_\phi^+(z) \equiv \frac{\gamma}{\omega\,\mu_0} A_+ \left\{\frac{1}{r}\right\} \exp\{-j\,\gamma\,z\} \exp\{j\omega t\}, \quad \text{(12.42)}$$

$$\gamma \equiv \sqrt{\omega^2\,\mu_0(\varepsilon' - j\,\varepsilon'')}\,. \quad \text{(12.43)}$$

If we include losses due to the conductivity of the metallic conductors (see details in the section on waveguides below), and if the losses are small, the coaxial propagation will be given by

$$E_r^{+\text{coax}}(z) = A_+ \left\{\frac{1}{r}\right\} \exp\{-j\,\gamma\,z\} \exp\{j\omega t\} \exp\{-\alpha_D z\} \exp\{-\alpha_M z\}, \quad \text{(12.44)}$$

$$H_\phi^{+\text{coax}}(z) \equiv \frac{\gamma}{\omega\mu} A_+ \left\{\frac{1}{r}\right\} \exp\{-j\,\gamma^{\text{coax}}\,z\} \exp\{j\omega t\} \exp\{-\alpha_D z\} \exp\{-\alpha_M z\}, \quad \text{(12.45)}$$

and

$$\gamma^{\text{coax}} \equiv \omega\sqrt{\mu_0\varepsilon'}, \quad \text{(12.46)}$$

where the attenuations factors for the coaxial structure due to the finite metal walls conductivity (α_M) and the imaginary part of the permittivity (α_D), are

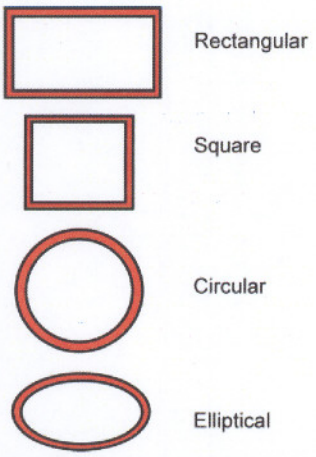

Fig. 12.14—Cross section of waveguide structures that cannot propagate TEM modes.

$$\alpha_M \equiv \frac{1}{2}\sqrt{\frac{\omega\,\varepsilon}{2\,\sigma_{mw}}}\,\frac{\left(r_b + r_a\right)}{\ln\left(\frac{r_b}{r_a}\right)\left(r_b\,r_a\right)} \qquad (12.47)$$

and

$$\alpha_D \equiv \frac{\gamma^{\text{coax}}\,\varepsilon''}{2\,\varepsilon'}\,. \qquad (12.48)$$

The coaxial cable metal losses will be a minimum for $(r_b / r_a) \cong 4$.

12.3.3 Waveguides. The waveguide metal structures, shown in Fig. 12.14, were developed for electromagnetic energy transmission in the microwave frequency range (3 to 300 GHz), in view of their small losses at these frequencies. The circular waveguides are potentially important for the excitation of reservoirs and wells.

The waves that can be transmitted along these systems have field components along the direction of propagation, here assumed as the z-axis. Transverse magnetic modes (TM) have zero H_z field components, and transverse electric field modes (TE) have zero E_z components. The propagation constant, γ, depends both on material properties (σ, ε, and μ_M of the enclosed material and σ_{mw} of the surrounding metal walls) and the dimensions of the waveguide. According to the value of the applied frequency, a given waveguide will either support waves that travel along the guide or attenuated waves (evanescent modes). We will examine the case of cylindrical waveguides in view of their importance in energy propagation in threaded oil pipes or in coil tubing.

12.3.4 Cylindrical Waveguide: TM Modes ($H_z = 0, \sigma = 0, \varepsilon'' = 0, \mu_M = \mu_0$, radius $= a$, $\sigma_{mw} = \infty$). The propagation constant for these modes is[75]

$$\beta_{n,m}^{TM} = \sqrt{\omega^2\mu_0\varepsilon - \frac{\left(p_{n,m}^{\text{TM}}\right)^2}{a^2}}\,. \qquad (12.49)$$

The constants $p_{n,m}^{\mathrm{TM}}$ arise from the imposed boundary conditions at the metal surfaces. The smaller values are $p_{0,1}^{\mathrm{TM}} = 2.405$, $p_{1,1}^{\mathrm{TM}} = 3.382$, and $p_{0,2}^{\mathrm{TM}} = 5.135$. For each root, we have a given mode of solution. According to the value of the frequency, the propagation constant will be real (propagation) or imaginary (evanescence). The cutoff frequency, ω_C, corresponds to the first value of ω, where propagation occurs (β real).

$$\omega_C^{TM} = \omega_{01}^{\mathrm{TM}} = \frac{2.405}{a\sqrt{\mu_0 \varepsilon}} . \quad \text{..... (12.50)}$$

12.3.5 Cylindrical Waveguides: TE Modes ($E_z = 0, \sigma = 0, \varepsilon'' = 0, \mu_M = \mu_0$, radius $= a$, $\sigma_{mw} = \infty$). The propagation constant for these modes is

$$\beta_{n,m}^{\mathrm{TE}} = \sqrt{\omega^2 \mu_0 \varepsilon - \frac{\left(p_{n,m}^{\mathrm{TE}}\right)^2}{a^2}} . \quad \text{..... (12.51)}$$

Again, the constants $p_{n,m}^{\mathrm{TE}}$ arise from the imposed boundary conditions at the metal surfaces.[75] The smaller values are $p_{1,1}^{\mathrm{TE}} = 1.841$, $p_{1,2}^{\mathrm{TE}} = 3.054$, and $p_{0,1}^{\mathrm{TE}} = 3.832$. For each root, we have a given mode of solution. According to the value of the frequency, the propagation constant is real (propagation) or imaginary (evanescence). The cutoff frequency for TE modes is

$$\omega_C^{\mathrm{TE}} = \omega_{11}^{\mathrm{TE}} = \frac{1.841}{a\sqrt{\mu_0 \varepsilon}} . \quad \text{..... (12.52)}$$

Thus, for cylindrical waveguides, the first mode to propagate is the TE_{11} mode because it has the lowest cutoff frequency. If the waveguide is empty or filled with materials with electrical properties similar to a vacuum (μ_0 and ε_0), this mode will have a cutoff wavelength $\lambda_{C0,\mathrm{TE}11} = 3.41a$. The situation for this and other modes is illustrated in Fig. 12.15.

12.3.6 Attenuation Caused by Metallic Walls. The above relations were obtained assuming infinite conductivity for the cavity walls $\sigma_{mw} = \infty$. In fact, real metallic walls have a finite conductivity, σ_{mw}, so that the waves will attenuate as they travel along the waveguides. The attenuations for TE and TM modes are

$$\alpha_{n,m}^{TE}(\sigma_{mw}) = \left\{ \frac{R_m}{aZ_0\sqrt{\left[1 - \frac{\left(k_{c,n,m}^{TE}\right)^2}{k_0^2}\right]}} \right\} \left\{ \frac{\left(k_{c,n,m}^{TE}\right)^2}{k_0^2} + \frac{n^2}{\left[\left(p_{n,m}^{TE}\right)^2 - n^2\right]} \right\} \quad \text{..... (12.53)}$$

and

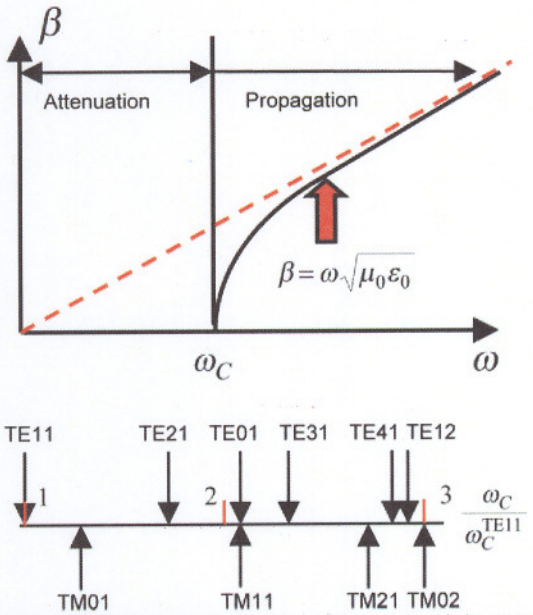

Fig. 12.15—The top graph shows transition between attenuation and propagation regions as a function of angular frequency (the dotted line indicates propagation dependence in the absence of the guide, in free space). The bottom sketch shows position of TE and TM modes for a cylindrical empty waveguide.

$$a_{n,m}^{\mathrm{TM}}(\sigma_{mw}) = \left\{ \frac{R_m}{aZ_0\sqrt{\left[1 - \frac{\left(k_{c,n,m}^{TM}\right)^2}{k_0^2}\right]}} \right\}, \quad \text{..... (12.54)}$$

where

$$R_m = \sqrt{\frac{\omega\mu_0}{2\sigma_{mw}}} \quad \text{..... (12.55)}$$

and

$$Z = \sqrt{\frac{\mu_0}{\varepsilon}}, \quad \text{..... (12.56)}$$

$$k_{c,n,m}^{TM} = \frac{p_{c,n,m}^{TM}}{a}, \quad \text{..... (12.57)}$$

$$k_{c,n,m}^{TE} = \frac{p_{c,n,m}^{TE}}{a}, \quad \text{..... (12.58)}$$

and $k_0 = \omega\sqrt{\mu_0\varepsilon}$. ..... (12.59)

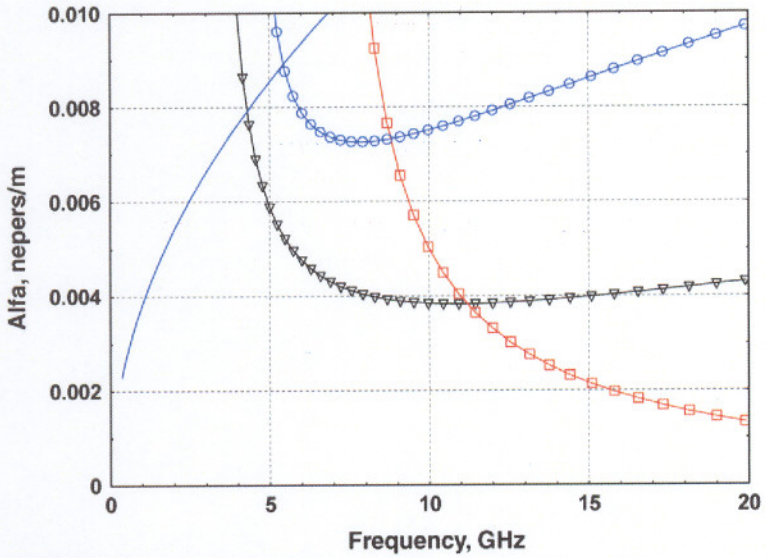

Fig. 12.16—*E, H* field attenuation (vertical axis) vs. frequency (horizontal axis) for a coaxial cable (continuous trace), TE01 mode (squares), TE11 dominant mode (triangles), and TM01 mode (circles). The wave guide and coaxial cable diameter is 2 in. The steel metal walls have a resistivity of 1.04×10^{-7} ohm/m.

These values of attenuation determine the wall losses for microwave energy transmitted along a pipe (this energy is transformed into heat) and the amount of power available at a distance, L, from the source. Fig. 12.16 shows the frequency dependence of the attenuation for modes TE11, TE01, and TM01 in an empty ($\mu_M = \mu_0, \varepsilon = \varepsilon_0, \sigma = 0$) circular waveguide of radius a. The figure also shows the attenuation for an equally empty coaxial cable with an external conductor with radius, a, and an internal conductor of radius, $a/4$.

The TE01 mode has an attenuation that decreases monotonically as the frequency increases, thus, indicating that this mode is convenient for transmission at high frequency. Transmitted power depends on (E,H) products so that the attenuation for power transmission doubles the field attenuation values.

Attenuation can be measured in nepers/m or in decibels, and the relationship between these units is

$$\text{attenuation (decibels/m)} = \text{attenuation (nepers/m)}\, 20 \log_{10}(e)$$
$$= 9.6858 \text{ attenuation (nepers/m)}. \quad \ldots\ldots\ldots\ldots\ldots\ldots \quad (12.60)$$

Fig. 12.17 shows the fraction of the power applied to a waveguide or a coaxial cable that will arrive at the end of a 1 km-long line. The waveguides are much better transmitters at higher frequencies. The power "lost" is converted into heat at the line metallic walls. As shown by the figure, waveguides are much better transmitters of power than coaxial cables at higher frequencies.

In both type of structures, the attenuation is caused by the induction of electrical currents at the surface of the metallic conductors. As these conductors have finite electrical conductivities, the flow of the induced currents results in power losses as in the case of any current-carrying wire. The power dissipated at the walls is, thus, conveniently converted into heat. By selecting a given frequency value, the ratio of power transmitted to power dissipated in the walls can be chosen at will.

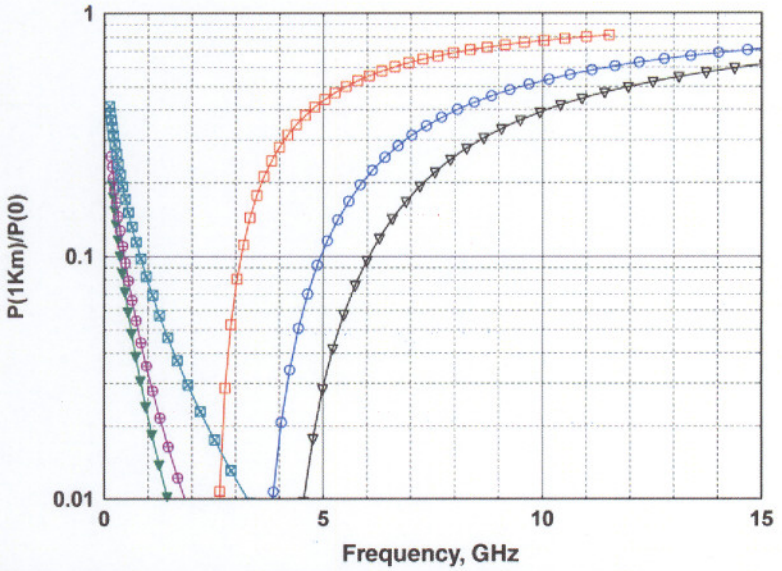

Fig. 12.17—Power ratio (vertical axis) at the depth of 1 km (3,000 ft) for different size wave guides (TE01 mode) and coaxial cables, as function of the applied frequency (horizontal axis): 6-in. diameter wave guide (empty squares) and coaxial (filled squares), 4.5-in. diameter wave guide (empty circles) and coaxial (filled circles), and 2-in. diameter wave guide (empty triangles) and coaxial (filled triangles). Losses, because of metal walls with a resistivity of 1.04×10^{-7} ohm/m, are the only losses considered.

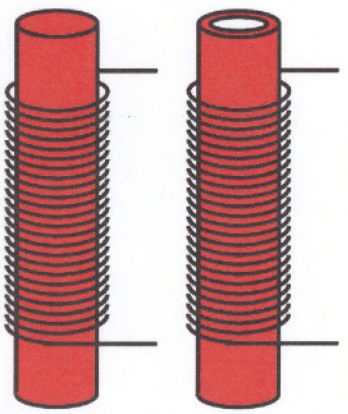

Fig. 12.18—The nature of an inductive heater: a metallic core is excited by the fields created by the current flowing in the coil. The core can be solid or a cylindrical metallic shell.

12.3.7 Inductive Concentrated Heaters. Inductive heating has been widely applied outside of the oil industry in steel foundries for light alloy melting (aluminum and magnesium), and in copper and zinc foundries.[5,6] It occurs when a metal core is excited by a coil of wire carrying an alternating current, as shown in Fig. 12.18. The metal is characterized by a high conductivity ($\sigma = 10^7$ siemens/m) and real permittivities and permeabilities ($\mu \cong \mu_0$, $\varepsilon \cong \varepsilon_0$).

For an applied magnetic field, H_0, in the z direction along the core axis, the electric and magnetic fields inside the solid core with radius a, are

$$H_z(r, t) = H_0 \frac{J_0(\gamma r)}{J_0(\gamma a)} \exp(j\omega t) . \quad (12.61)$$

$$E_\phi(r, t) = H_0 \frac{\gamma}{\sigma} \frac{J_1(\gamma r)}{J_0(\gamma r)} \exp(j\omega t) . \quad (12.62)$$

J_0 and J_1 are Bessel functions of complex arguments. Since the applied frequency, ω, is chosen so that $\sigma >> \omega\varepsilon_0$, we have

$$\gamma^2 \cong \{-j\omega\sigma\mu_0\} . \quad (12.63)$$

The real time-averaged power entering the core at $r = a$ (in the $-r$ direction) is

$$P_{\text{real}}(a) = -(H_0)^2 \text{Re}\left[\frac{\gamma}{2\sigma} \frac{J_1(\gamma a)}{J_0(\gamma a)}\right] \equiv +(H_0)^2 \text{Re}\left\{\frac{j\omega\mu_0 a}{4}[\mu_R]\right\} \quad (12.64)$$

and

$$\mu_R \equiv \left[\frac{2}{\gamma a} \frac{J_1(\gamma a)}{J_0(\gamma a)}\right] \equiv [\mu'_R - j\mu''_R] . \quad (12.65)$$

In terms of an effective relative permeability, μ_R, refer to **Fig. 12.19**.[76,77] The real power per unit area, input to the core, is

$$P_{\text{real}}(a) = +(H_0)^2 \left\{\frac{\omega\mu_0 a}{4} \mu''_R\right\} . \quad (12.66)$$

The real power per unit area grows as $(\omega)^{1/2}$ at high frequency, and as the frequency grows, the power is more concentrated near the core surface, as shown in **Fig. 12.20**. Thus at high frequencies, the heating occurs closer to the surface.

12.3.8 Energy Gain in Electrical Heating Processes Used in Enhanced Oil Production. It is important to consider the energy gain (EG) of the particular electrical heating system used in enhanced oil recovery. If the production is increased by (ΔQ) barrels per day, under the effect of P_E kW of electrical power (generated from a process with energy efficiency, η), we define the energy (or power) gain, EG, as

$$\text{EG} \equiv \frac{68.366(\Delta Q)}{P_E}\eta, \quad (12.67)$$

where η is of the order of 30% for thermal electrical energy generation, 85% for hydroelectric generation, and 15% for microwave generation. The efficiency factor, η, represents the ratio of the 60 Hz electrical energy produced in a given process (thermal/hydroelectric) to the energy input in each process. Electrical energy in the microwave range is produced from 60 Hz electrical energy with an approximate efficiency of 50%.

The factor 68.366 comes from the equivalence of 1 standard bbl of oil with 5.6 million Btu as heating content and the equivalence of 1 kW-h = 3,413 Btu.[78] Thus, 1 bbl of oil per day is

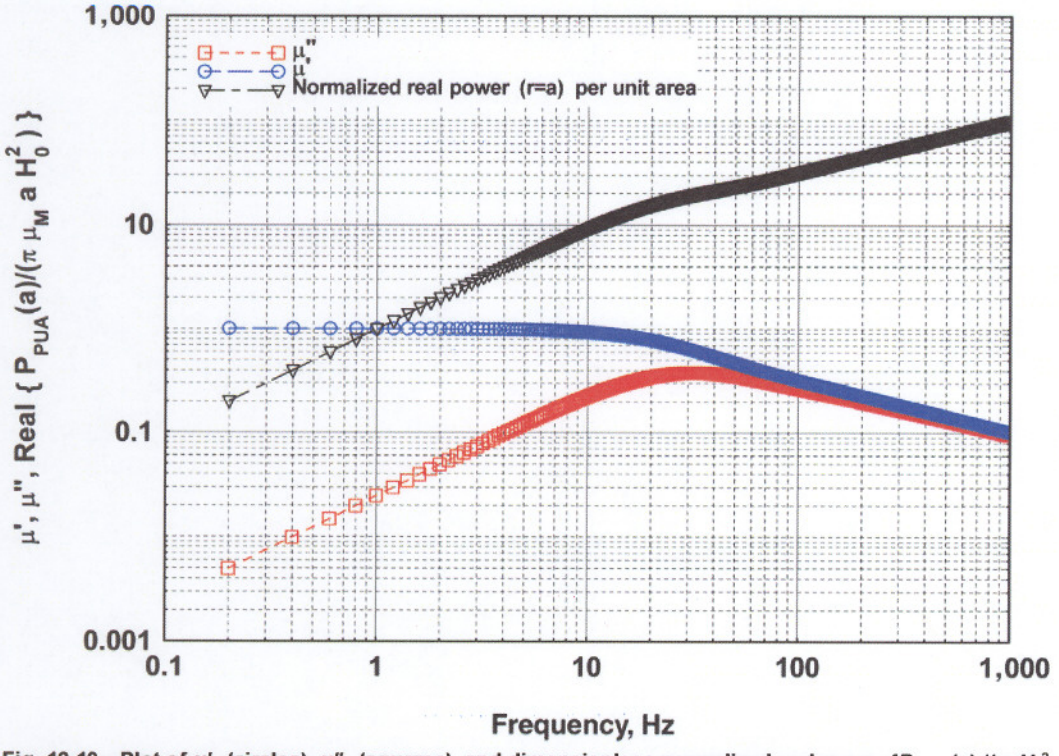

Fig. 12.19—Plot of μ'_R (circles), μ''_R (squares), and dimensionless normalized real power $\{P_{PUAl}\ (a)\ /(\pi\ H_0^2\ a\ \mu_0\}$ (triangles) as functions of frequency for a metallic cylinder with radius = 0.05 m, conductivity = 10^{+7}, and $\mu_M = \mu_0$.

equivalent to 68.366 kW. For the different types of electrical power generation processes, the different energy gains will be approximately

$$EG_{Thermal} = \frac{20\Delta Q}{P_E},\ EG_{Hydro} = \frac{58\Delta Q}{P_E},\ EG_{Microw} = 0.5\ EG_{Thermal} = 0.5\ EG_{Hydro} \cdot \ldots \quad (12.68)$$

The energy (or power) gain concept is useful in the relative evaluation of different electrical heating systems and the comparison of electrical heating with steam injection characterized with EG < 10.* For more details, refer to the chapter on steam injection in the Reservoir Engineering and Petrophysics section of this *Handbook*.

Because electrical heating is considered as a viscosity reduction process for the production of heavy and extra-heavy oil, it is very pertinent to compare the energy efficiency of this process with steam injection—perhaps the more accepted process used in the industry for the production of hydrocarbon during the last four decades.

12.3.9 Sources of Dielectric Losses. In the electrical heating of oil wells or reservoirs, we can disregard magnetic losses (including those in the metallic structures) because $\mu \cong \mu_0$. The power dissipated in a given volume, V, is then given by

* Personal communication with H. Mendoza, PDVSA Production and Exploration Division, Lagunillas, Venezuela (1998).

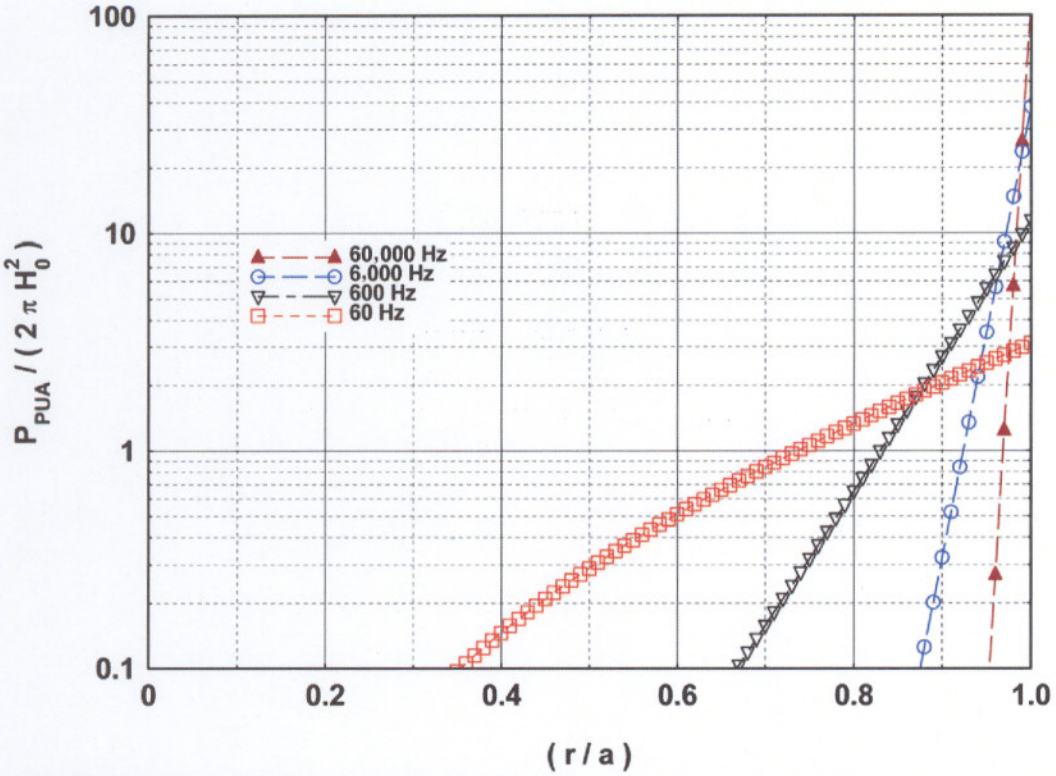

Fig. 12.20—Plot of normalized real power per unit area {P_{PUA} (*r*) / (2 μ H_0^2)} as a function of (*r/a*), showing the frequency dependence of the spatial distribution of dissipated power in a metallic cylinder at different frequencies *f*: *f* = 60,000 Hz (triangles); *f* = 6,000 Hz (circles); *f* = 600 Hz (inverted triangles); and *f* = 60 Hz (squares). The metal cylinder has a radius of 0.05 m, conductivity = 10^{+7}, and $\mu_M = \mu_0$.

$$\text{Power} = \left(\frac{1}{2}\right)\int dV\left[\omega\,\varepsilon''(\omega) + \sigma(\omega)\right] |\,E\,|^2 \,. \qquad (12.69)$$

Losses, because of the presence of $\varepsilon''(\omega)$, are defined as dielectric losses. They are caused by several processes: electronic, ionic or atomic, orientation, and space charge or interfacial.[79] All the processes occur because of the electrical field influence on the charge distributions existing in matter. The nature of these mechanisms is sketched in **Fig. 12.21**.

Mechanisms (a) and (b) imply field-induced dipoles, while (c) occurs in polar systems with permanent dipolar structures. Process (d) occurs because of complex charge distributions at interfaces (as between a solid and a liquid). Each of these mechanisms implies energy losses caused by "frictional" forces as the dipoles follow the changes in the electric field. The losses occur in different frequency ranges as shown schematically in **Fig. 12.22**.[67,68] Losses in the microwave frequency range occur either because of the presence of polar molecules (like water) or possible complex space charge effects.

Because petroleum (without water) is a collection of mostly nonpolar molecules, it is practically transparent to electromagnetic energy in all the frequency ranges ($\varepsilon'/\varepsilon_0 = 2$ to 4, $\varepsilon'' \cong 0$). The situation is different in a reservoir where water is associated with a solid matrix, either absorbed in material capillaries, adsorbed on grain surfaces, or is chemically associated to other molecules. The resonance of bound water occurs at lower frequencies than the free-water resonance that occurs near 20 GHz at room temperature.

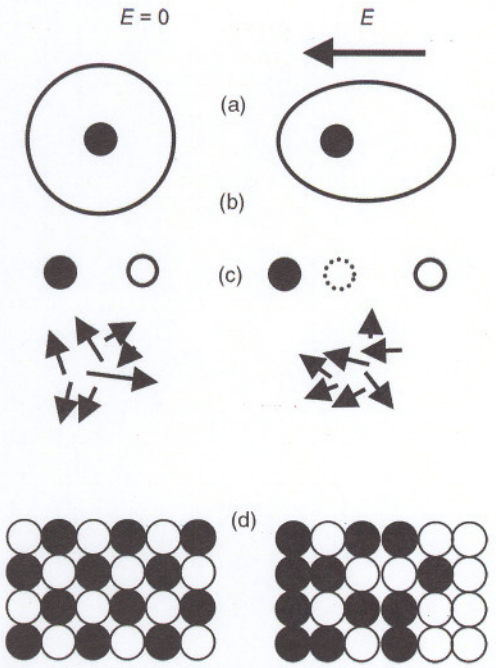

Fig. 12.21—Polarization mechanisms: (a) electronic, (b) ionic, (c) dipolar, and (d) interfacial or space polarization. Filled black circles represent positive charges while white circles represent negative charges. Arrows indicate permanent dipoles. Dashed circles represent displaced charges.

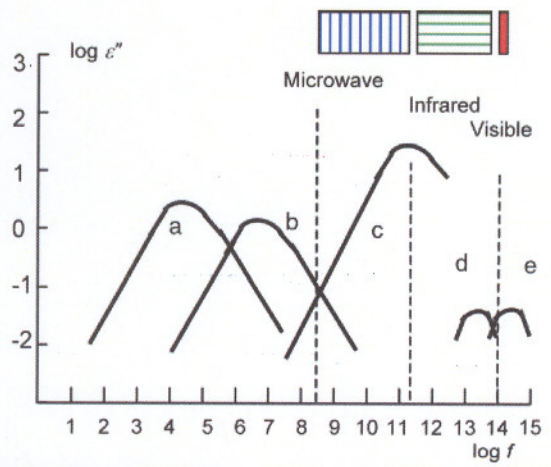

Fig. 12.22—(a) interfacial polarization, (b) water in a material matrix, (c) free liquid water, (d) ionic polarization loss, (e) electronic polarization losses.

The basic curve for each resonance is given by the derivation because of Debye, in terms of relative permeabilities at zero frequency and at very large frequencies, and a time constant, τ,

$$\varepsilon(\omega) = \varepsilon'(\infty) + \frac{\varepsilon'(\infty) - \varepsilon'(0)}{1 + j\,\omega\,\tau} \quad \text{..... (12.70)}$$

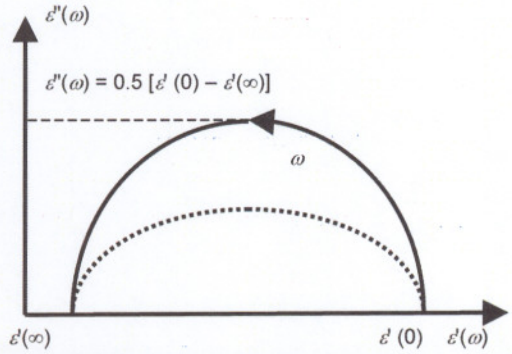

Fig. 12.23—Cole-Cole plot of the simple Debye model of dielectric losses in terms of a single time constant (continuous curve) and multiple time constants (dotted curve).

The previous expressions yield a semicircular Cole-Cole plot, as shown in Fig. 12.23, similar to the plot for a parallel combination of a capacitance and a resistance. The dotted ellipse shows the behavior generally found experimentally. This behavior is interpreted as being caused by the contribution of several time constants.

12.4 Fluid Flow Modeling Considerations

In the modeling of any system, one is always faced with the dilemma of choosing the level of complexity that correctly predicts the response of interest. In the case of modeling the electrical heating of wells and reservoirs for heavy or extra-heavy oil at low frequencies (below the microwave range) and considering only one liquid phase and no gas phases, the systems of equations shown in this section are considered sufficient. The problem is still unsolved for the case of microwave heating of reservoirs, in which a complete model, which correctly takes into account the electric losses of a system of solid grains, liquids with dissolved gases and salts (with the corresponding complex geometrical, scaling, and electrochemical properties in the presence of electrical diffusion currents and space charges), is not yet available. For the case of concentrated heating (either resistive or inductive) and distributed heating in the reservoir and surrounding regions (at frequencies below the microwave range) or distributed heating in the metal elements (at any frequency) the equations given next (in a cylindrical coordinate system) are deemed sufficient.

12.4.1 Thermal Processes. Heat energy flow per unit area and per unit time ($\vec{Q}_T$) in the presence of forced convection because of a velocity, $\vec{V}$, is given by

$$\vec{Q}_T = -K_T\,\vec{\nabla}T + \rho\,C_P\,\vec{V}\,T, \quad (12.71)$$

where K_T is the thermal conductivity, ρ is the density of the liquid, and C_P is the specific heat at constant pressure.[80] In the presence of dissipation of power, an energy balance is described by

$$\vec{\nabla}^2 T - \frac{1}{\kappa_T}\vec{\nabla}\cdot\vec{\nabla}\left(\vec{V}\,T\right) = \frac{1}{\kappa_T}\frac{\partial T}{\partial t} - \frac{1}{K_T}P_{\text{PUV}} \quad (12.72)$$

in terms of κ_T the thermal diffusivity, and P_{PUV} the dissipated power per unit volume (electrical in our case). Thus, in a cylindrical coordinate system with axial symmetry with respect to the z axis, the differential equation for a region of spatially constant parameters is

$$\frac{\partial^2 T}{\partial r^2}+\frac{1}{r}\frac{\partial T}{\partial r}+\frac{\partial^2 T}{\partial^2 z}-\frac{1}{K_T}\left(V_r\frac{\partial T}{\partial r}+V_z\frac{\partial T}{\partial z}\right)$$
$$-T\left(\frac{\partial V_r}{\partial r}+\frac{\partial V_z}{\partial z}\right)=\frac{1}{\kappa_T}\frac{\partial T}{\partial t}-\frac{1}{K_T}P_{\mathrm{PUV}}. \quad \text{(12.73)}$$

The third term on the left, the product of temperature multiplied by the divergence of the velocity, has been neglected in many models of heating of reservoirs (it is strictly zero only for incompressible fluids.).

12.4.2 Fluid Flow in the Porous Media. The fluid flow equation in the porous media of the reservoir, deemed to be representative of solution-gas-drive production mechanisms, is

$$\frac{\partial^2 P}{\partial r^2}+\frac{1}{r}\frac{\partial P}{\partial r}+\frac{\partial^2 P}{\partial^2 z}=\frac{c\,\phi\,\mu}{k}\frac{\partial P}{\partial t}, \quad \text{(12.74)}$$

where P is the pressure, $\mu(T)$ is the temperature-dependent viscosity, k is the permeability, c is the compressibility, and ϕ is the porosity.[81–83] The fluid velocity, V (we assume that only oil is present) has the following components:

$$V_r=-\frac{k}{\mu}\frac{\partial P}{\partial r}. \quad \text{(12.75)}$$

$$V_z=-\frac{k}{\mu}\frac{\partial P}{\partial z}. \quad \text{(12.76)}$$

The mass fluid flow per unit area, $\vec{Q}_m$, and the temperature-dependent kinematic viscosity, v, are given by

$$\vec{Q}_m=\rho\vec{V} \quad \text{(12.77)}$$

and

$$v(T)=\frac{\mu(T)}{\rho}. \quad \text{(12.78)}$$

12.4.3 Electrical Processes. In the case of concentrated resistive heating, where a sinusoidal current of root mean square (RMS) magnitude I ($I_{\max}=I\sqrt{2}$) flows through a wire resistance of resistance, R, the total power dissipated is I^2R. The power per unit volume is uniform over the volume of the resistor if the skin depth is much larger than the wire radius. The skin depth δ_S indicates how far the electromagnetic fields penetrate in a material with conductivity σ, and it is given by

$$\delta_S=\sqrt{\frac{2}{\omega\mu_M\sigma}}. \quad \text{(12.79)}$$

The behavior of the skin depth, as a function of frequency, is shown in Fig. 12.24 for typical resistance materials (nickel-chrome alloys with conductivity 10^7 siemens/m). As the frequency increases, we reach the inductive heating regime previously discussed.

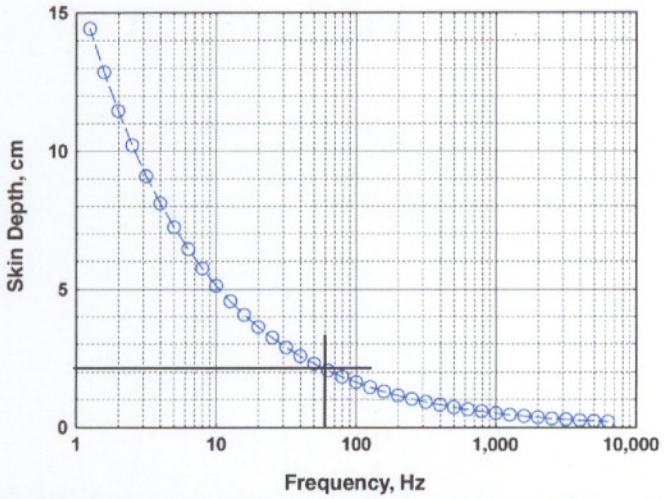

Fig. 12.24—Plot of skin depth in cm vs. frequency in Hz for nickel-chrome alloys. The crossing straight lines indicate that at 60 Hz, the skin depth is of the order of 2 cm, much larger than the diameter of heating wires.

In the case of low-frequency heating distributed over the reservoir and the under and overburden regions, the conductivities of the materials involved, are much smaller than metallic conductivities (0.1 to 0.02 siemens/m), the corresponding skin depths are large over the volume elements considered in a given model. Thus, the determination of dissipated energy per unit volume can be obtained from the solution of Maxwell's equations in the low-frequency limit where

$$\vec{\nabla} \times \vec{E} > > j\omega\mu\vec{H}, \Rightarrow \vec{\nabla} \times \vec{E} \simeq 0 \quad \text{..... (12.80)}$$

so that we can define a scalar potential Φ

$$\vec{E} = -\vec{\nabla}\Phi \quad \text{..... (12.81)}$$

with the current density

$$\vec{J} = \left(\sigma + j\,\omega\,\varepsilon_0\right)\vec{E} \; . \quad \text{..... (12.82)}$$

Thus, each volume element, shown in Fig. 12.25, can be represented by resistances and capacitances connecting to other volume elements. The resulting distributed circuit is shown in Fig. 12.26, and the component conductance and capacitance values are given next.[47]

$$Yz = \frac{\pi\,\sigma\left(rd^2 - rc^2\right)}{(\Delta z)} \; ; \quad Yr = \frac{2\,\pi\,\sigma(\Delta z)}{\ln\left(\frac{rb}{ra}\right)} \; . \quad \text{..... (12.83)}$$

$$Cz = \frac{\pi\,\varepsilon_0\left(rd^2 - rc^2\right)}{(\Delta z)} \; ; \quad Cr = \frac{2\,\pi\,\varepsilon_0(\Delta z)}{\ln\left(\frac{rb}{ra}\right)} \; . \quad \text{..... (12.84)}$$

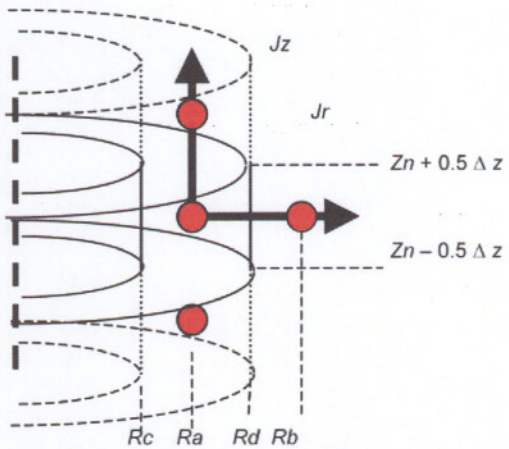

Fig. 12.25—Space discretization in cylindrical coordinates.

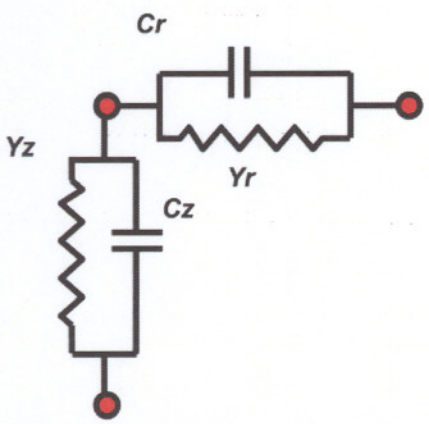

Fig. 12.26—Elements for the distributed circuit for current conduction.

For the frequencies involved in distributed resistive heating at 60 Hz or lower frequencies, the capacitances are neglected. For a given current (or currents) applied at given nodes, the circuit can be solved for all the node voltages by applying Kirchhoff's current law (KCL), requiring that the sum of all the currents that flow into a node should vanish (charge conservation).

Although not necessary to solve the problem, an equivalent circuit approach can be used for visualizing (and calculating) the solutions of the temperature and fluid flow equations.[46,47,50,51,84] It is particularly helpful in treating regions with space varying parameters. For the volume elements of Fig. 12.25, the equivalent circuits for fluid flow in porous media and for heat transfer with convection are shown in **Figs. 12.27 and 12.28**.

In the absence of gravity effects, the element values for the fluid flow are

$$YVz = \frac{\pi k \left(rd^2 - rc^2\right)}{\mu(T)(\Delta z)}\ ;\ YVr = \frac{2\pi k\,(\Delta z)}{\mu(T)\ \ln\left(\frac{rb}{ra}\right)}, \quad \text{..... (12.85)}$$

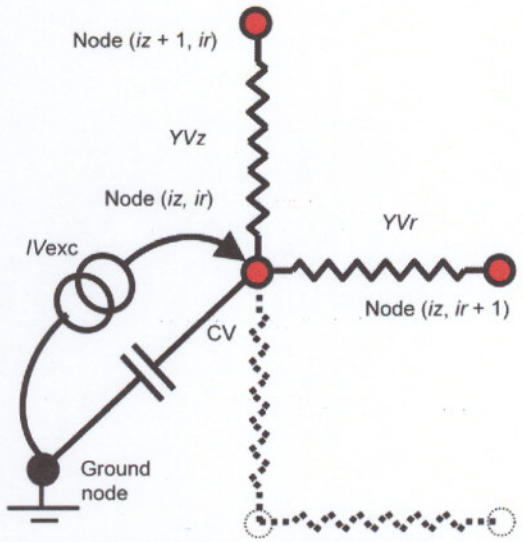

Fig. 12.27—Elements for the distributed circuit for fluid flow in porous media.

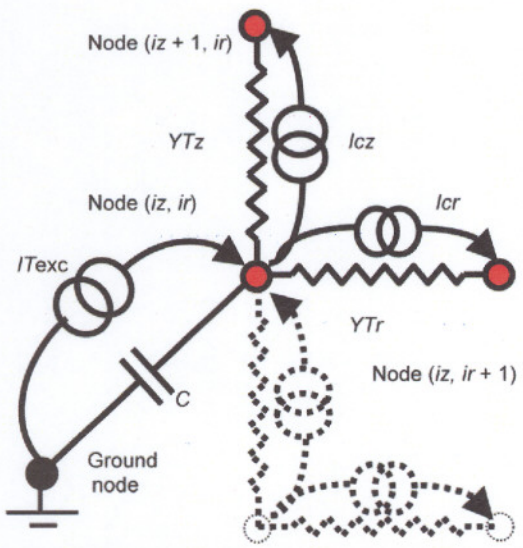

Fig. 12.28—Elements for the distributed circuit for thermal conduction with convection in the positive *r* and *z* directions.

$$CV = c\,\phi\,\pi\left(rd^2 - rc^2\right)(\Delta z), \quad \text{..... (12.86)}$$

and

$$IV\text{exc} = \left[P\left(z, r, 0^-\right)c\,\phi\right]\pi\left(rd^2 - rc^2\right)(\Delta z), \quad \text{..... (12.87)}$$

where the excitation current (IVexc) introduces the initial pressure conditions for the problem.

The element values for the thermal case are equivalent admittances, capacitances, and convection currents

$$YTz = \frac{\pi K_T \left(rd^2 - rc^2\right)}{(\Delta z)} \; ; \quad YTr = \frac{2\pi K_T(\Delta z)}{\ln\left(\frac{rb}{ra}\right)}, \qquad (12.88)$$

$$CT = \frac{K_T}{\kappa_T}\pi\left(rd^2 - rc^2\right)(\Delta z), \qquad (12.89)$$

$$Icz = V_z \frac{K_T \pi\left(rd^2 - rc^2\right)}{\kappa_T} \; ; \quad Icr = V_r \frac{K_T 2\pi (rb\Delta z)}{\kappa_T}, \qquad (12.90)$$

and

$$IT\text{exc} = \left[\frac{K_T}{\kappa_T} T\left(z, r, 0^-\right) + P_{\text{PUV}}\right]\pi\left(rd^2 - rc^2\right)(\Delta z), \qquad (12.91)$$

where the excitation current (ITexc) introduces the initial temperature conditions for the problem and the applied power per unit volume.

The circuital approach is particularly convenient in the case of problems covering regions with different properties. For example, the fluid flow equation for porous media originates from a mass balance of

$$\vec{\nabla}\left(\rho \, \vec{v}\right) = -\frac{\partial(\phi \, \rho)}{\partial t}, \qquad (12.92)$$

which, assuming spatially independent compressibility and porosity, yields

$$\vec{\nabla} \cdot \left[\frac{k}{\mu(T)} \vec{\nabla} P\right] = c \, \phi \frac{\partial P}{\partial t}, \qquad (12.93)$$

which gives the equation indicated at the beginning of this section, only if k and $\mu(T)$ are space independent. In the case of reservoir heating, if the temperature is space-dependent, the equation for flow in fluid media becomes

$$\vec{\nabla} \cdot \left(\frac{k}{\mu\{[T(r, z)]\}} \vec{\nabla}^2 P\right) + \vec{\nabla} P \cdot \vec{\nabla}\left(\frac{k}{\mu\{[T(r, z)]\}}\right) = c\phi \frac{\partial P}{\partial t} \; . \qquad (12.94)$$

12.4.4 Fluid Flow in the Well. For steady laminar flow of a single-phase fluid, the velocity of the fluid in the well pipe directed along the z axis, of radius R_{well} is given by the Hagen-Poisseuille relation, which is written as

$$V_z = -\frac{\left(R_{\text{well}}\right)^2}{8\mu(T)} \frac{\partial P}{\partial z} \; . \qquad (12.95)$$

12.4.5 Model Response For Vertical Wells: Concentrated Heating vs. Distributed Heating. We conclude this section with calculations comparing transient concentrated heating vs. dis-

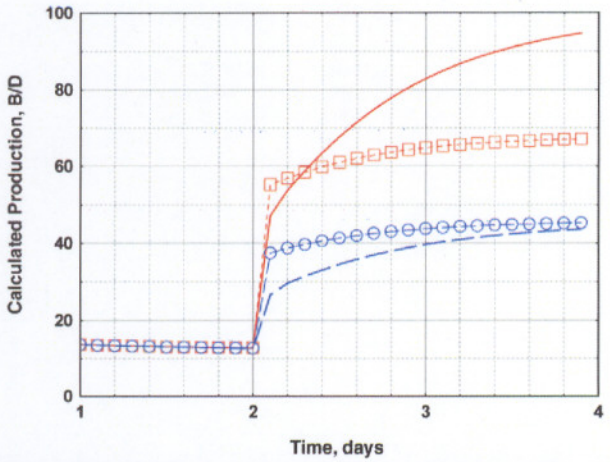

Fig. 12.29—Calculated production in B/D vs. time in days: 10 kW distributed heating (dashed line), 20 kW distributed heating (continuous line), 10 kW concentrated heating (circles), 20 kW concentrated heating (squares). No limitations of temperature are imposed. Heating is applied at time, t = 2 days.

tributed low-frequency (60 Hz) heating (according to scheme (b), shown in Fig. 12.4) for reservoir and well conditions, such as those given in the test case for the Tia Juana field in western Venezuela.[85]

Fig. 12.29 shows the production response for both cases of heating at different power levels. It is interesting to see that at low power levels concentrated and distributed heating yield similar responses. As the applied power increases, the distributed heating case shows a better response, although it takes a few more days to reach steady state. In any case, the response is quick, as indicated in most of the field test cases reported.

Fig. 12.30 shows the production response for both cases of heating at a 30 kW power level. The concentrated heating cases shown correspond to power applied under different control temperature conditions at the heater. If the temperature exceeds a set point (85°C), the heater is turned off and then restarted if the temperature decreases. The figure determines the importance of reporting real field conditions to properly evaluate the different energy gains.

Fig. 12.31 shows the behavior of the temperature as a function of time. The temperature decrease, observed for the concentrated heating, is because of the increased convection cooling as the production increases. The energy gains determined from the numerical results in those cases with no temperature limitations are summarized in Table 12.2.

Additionally, one might note that many control systems for the electrical heating supplies use nonlinear devices (like silicon control rectifiers) that change the nature of the applied power sinusoidal waves so that the harmonic content of the applied voltage (or current) waveforms requires specialized watt meters for the correct evaluation of the applied power levels. The harmonic content implies that excitations at frequencies differing from the fundamental are present.

12.5 Field Tests

With few exceptions, we report only the field cases in which applied power was reported together with the oil production increase so that we can evaluate and compare the energy gains of the different processes tested.

12.5.1 Southwest Texas Proprietary Lease. ***Data Reported by Gill.***[16] Year: 1983; type of heating: distributed heating LF (60 Hz); depth of reservoir: 3,000 ft; oil type: paraffinic and

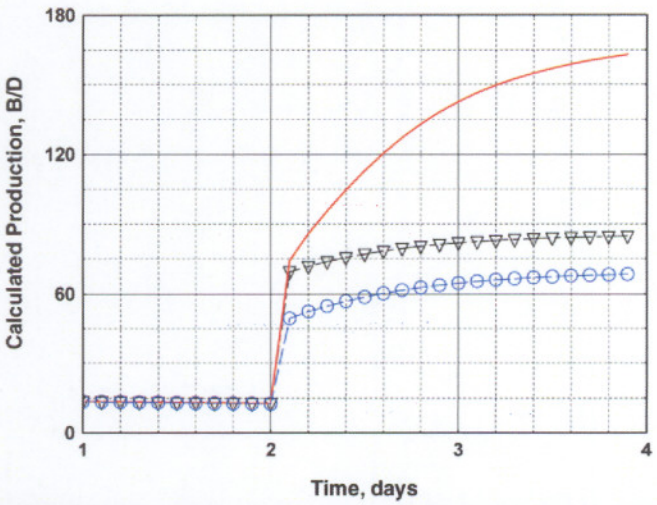

Fig. 12.30—Calculated production in B/D vs. time in days: 30 kW distributed heating with no temperature limitations (continuous line), 30 kW concentrated heating with no temperature limitations (triangles), and 30 kW concentrated heating with heater temperature set at 85°C (circles).

TABLE 12.2—ENERGY GAINS DETERMINED FROM NUMERICAL CALCULATIONS (AFTER TWO DAYS OF HEATING)

Applied power	10 kW	20 kW	30 kW
EG for distributed heating	66	84	102
EG for concentrated heating	66	55	49

asphaltic, 11°API; initial production: 0 B/D; final production: 76 B/D with 150 kW applied and 10 B/D with 12 kW; energy gain: 20 × 76/150 = 40 and 20 × 10/12 = 17.

12.5.2 Eastern Utah (Small Independent Company). ***Data Reported by Gill.***[16] Year: 1983; type of heating: distributed heating LF (60 Hz); depth of reservoir: 2,800 ft; oil type: paraffinic and asphaltic, 22°API; initial production: 4 BOPD, 25 BWPD; final production: 50 BOPD and 10 BWPD with 60 kW; energy gain: 20 × 46/60 = 15.

12.5.3 Oil Shales, Avintaquin Canyon, Utah. ***Data Reported by Sresty.***[20] Year: 1980; type of heating: distributed HF (5 to 20 kW at 13.56 MHz) applied to electrode systems inserted in the formation; surface deposits (1 m^3 excited); final production: 20 gal during a time not specified; energy gain: cannot be computed.

12.5.4 Tar Sands, Asphalt Ridge, Utah. ***Data Reported by Sresty.***[20] Year: 1981; type of heating: distributed HF (40 to 75 kW at 13.56 MHz) applied to electrode systems inserted in the formation; surface deposits (25 m^3 excited); initial production: 0; final production: 8 bbl over a 20-day test period; energy gain: 20 × (8/20)/40 = 0.2.

Comments. The EG calculation assumes that the power reported is the 60 Hz power of the HF power supply.

12.5.5 South Central Oklahoma. ***Data Reported by Gill.***[16] Year: 1983; type of heating: distributed heating LF (60 Hz); depth of reservoir: 7,200 ft; oil type: 11°API; initial production:

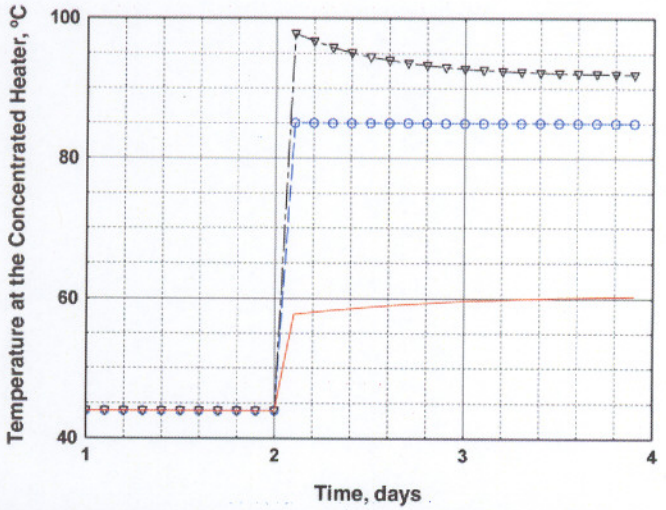

Fig. 12.31—Temperature in °C at the concentrated heater (located in the well at reservoir depth) vs. time in days: 30 kW distributed heating with no temperature limitations (continuous line), 30 kW concentrated heating without temperature limitations (triangles), 30 kW concentrated heating with heater temperature set at 85°C (circles).

20 BOPD, with concurrent diluent injection; final production: 50 B/D with 56.6 kW and 80 B/D with 100 kW; energy gain = 20 × 30/56.6 = 10.6 and 20 × 60/100 = 12.

12.5.6 Rio Panon, Brazil (Petrobras). ***Data Reported by Pizarro and Trevisan.***[38] Year: 1987; type of heating: distributed LF 60 Hz (well to well); depth of reservoir: about 1,000 ft; net pay zone thickness: 28 ft; permeability: 4 darcies; porosity: 27%; oil type: density 0.9612; viscosity: 2,500 cp at reservoir conditions; bottomhole temperature: 37.7°C; bottomhole pressure: 284 psi; initial production: 1.2 B/D; final production: 6.3 B/D at 20 kW and 12.6 kW at 30 kW; energy gain: 20 × (5.1)/20 = 5.1 and 20 × 11.4/30 = 7.6.

Comments. Test stopped after 70 days of heating because of voltage control system problems.

12.5.7 Sparky Formation, Frog Lake, Canada (Well Owned by Mazzei Oil and Gas Ltd.). ***Data Reported by Vinsome et al.***[17] Year: 1988; type of heating: distributed LF (2 to 60 Hz) with isolated sections of casing and production tubing with downhole temperature control); depth of reservoir: 1,270 ft; net pay zone thickness: 18 ft; porosity: 0.25 to 0.35; oil type: 11.5°API; viscosity: 10,000 cp; initial production: 18.8 B/D; final production: 75.4 B/D with average power of 15 kW; energy gain: 20 × (56.6)/15 = 75.5.

12.5.8 Lloydminster Heavy Oil Reservoirs (Tests at Wildemere, Northminster and Lashburn). ***Data Reported by Davison.***[86] Year: 1989/1990; type of heating: distributed LF (60 Hz) with isolated casing and downhole temperature control, and tubing heating at Lashburn; oil type: 11.4°API; initial production: 25 B/D (Lashburn); final production: 69 B/D with 15.5 kW (reservoir heating) and 50.3 B/D with 24 kW (wellbore heating); energy gain: 20 × 44/15.5 = 56.7 (reservoir heating) and 20 × 25.3/24 = 21 (borehole heating).

Comments. Failure of the projects at Northminster and Lashburn because of casing insulation failures and because of reservoir problems at Wildemere.

12.5.9 Wells JOC-570 and 571, Jobo Field (Near Morichal Eastern Venezuela) of Lagoven-PDVSA. ***Data.*** Year: 1992/1993; type of heating: distributed heating LF (less than 60 Hz one

phase with isolated sections of casing and production tubing with downhole temperature control); depth of reservoir: 3,800 ft; net pay zone thickness: 44 ft; resistivity 500 ohm/meter, 22% water; initial production: JOC-570 125 B/D (with concurrent diluent injection); final production (JOC-570 with 50 kW and concurrent diluent injection): 470 B/D with a 9 strokes per minute (SPM) pump, and 240 B/D with a 6 SPM pump; energy gains (JOC-570): 20 × (470–125)/50 = 138 and 20 × (240–125)/50=46; initial production: JOC-571 175 B/D (with concurrent diluent injection); final production: JOC-571 200 to 350 B/D average and 275 B/D after heating at 30 kW for a very few days); energy gain: JOC-571 20 – (275–175)/30 = 67.

Comments. Both wells were badly sanded, and operations were suspended. There was a history of short circuits and power supply problems (casing isolation failure suspected).

12.5.10 Dagang Oil Field, China, Well Zao 1269-2. ***Data Reported by Cheng et al.***[22] Year: 1995; type of heating: LF distributed resistive heating in metallic cable along hollow pump rods (cable length 2,850 ft) LF; depth of reservoir: 5,898 ft; oil type: heavy; bottomhole temperature: 87°C; initial production: 31.5 B/D; final production: 94.5 B/D with 44.8 kW applied; energy gain: 20 x 63/44.8 = 28.

Comments. Several wells were reported with no applied power specifications.

12.5.11 Frog Lake, 80 km North of Lloydminster, Alberta, Canada. ***Data Reported by McGee et al.***[87] Year: 1995; type of heating: distributed resistive LF (60 Hz) in vertical wells and from horizontal to vertical wells; depth of reservoir: 1,500 ft; net pay zone thickness: 9 to 15 ft; permeability: 2 darcies; porosity: 35%; oil type: 10–14°API; bottomhole temperature: 20°C; bottomhole pressure: 2,758 KPa.

Comments. Various types of problems affected the results—mainly sanding. Cable base systems, to deliver current to bottom of vertical wells, required a pump location several joints above the pay-zone. This required use of a tail pipe below the pump, which became filled with sand over time. Problems with downhole thermocouple measurements (possibly short circuits) led to the elimination of this downhole measurement. The tubing was used for current transport, but then, the wellhead operated at high voltages. The response of vertical wells suggested production increases. Horizontal well production did not increase but rather decreased because of the pump inability to produce the fluids accumulated, since the elements of the electrical system added to the original completion restricted the available space. The tests proved the possibility of a floating electrical connection between wells.

12.5.12 Tia Juana Field (Western Venezuela), Well LSE 4622 of Maraven-PDVSA. ***Data.*** Year: 1997; type of heating: concentrated resistive LF (30 kW fed by three-phase 480 volt rms) rated at 200°F with downhole temperature control; depth of reservoir: 1,040 ft; net pay zone thickness: 100 ft; permeability: 2 darcies; porosity: 35%; oil type: asphaltic 10°API; viscosity: 19,000 cp at 110°F; bottomhole temperature: 110°F; bottomhole pressure: 350 psi; initial production: 20 B/D; final production: 40 B/D; energy gain: 20 × 20/30=13.3.

12.6 Summary

The advantages of electrical stimulation of wells and reservoirs are several:

- The production is not interrupted by the application of electrical power.
- It seems more efficient energetically than steam stimulation (although more careful determinations of the energy gain factors should be obtained from fully instrumented field tests).
- It can be used in shallow wells where steam breakthrough can occur.
- Electrical heating does not require the additional investments required for a steam distribution system because most wells with pumps already have electrical grid connections. In most cases, the level of electrical power available at the well sites are sufficient to accommodate a higher power requirement.

• The widespread application of electrical submersible pumps (operating at high voltages) has generalized the knowledge required for electrical cable installations in oil installations, making it a routine process.

Further considerations on electrical heating are:

• The use of electricity, generated in plants that use fossil fuels, to increase oil production may seem contradictory, but it certainly should be used if it is energetically more efficient than steam stimulation.

• Many concentrated resistive heaters have been installed without temperature control. As the temperature increased because of gas flow (for example), the heaters failed. The required additional connections to downhole temperature detectors (metal resistances or thermocouples) complicate the installation of these heaters but their use is necessary.

• Distributed heating has been associated with the need for isolated sections of casing and production tubing (epoxy filled fiberglass structures), which are inherently weak under regular oil field usage. Additionally, water slug flow may tend to short-circuit some of these systems with the corresponding failures.

• Distributed resistance heating, although originally considered for high-frequency excitations, is in fact mostly used at a low-frequencies (close to 60 Hz).

• Very few modeling studies compared the transient response of concentrated vs. distributed heaters (and certainly no field comparison of the two methods has been carried out under similar conditions).

• Electrical heating requires a multidisciplinary approach, and many producers limit electrical engineering personnel activities to power generation and distribution. The application of electrical heating in the oil industry, if at all considered, is not a significant topic covered in electrical engineering university programs. This is so even in those countries where the economy depends significantly on heavy and extra-heavy oil production.

12.7 Future Technology Development

Although distributed low-frequency (60 Hz) heating critically depends on isolated casing and tubing sections (with doubtful field behavior), new connection designs and the development of new materials should improve the potential of this application.

Concentrated low-frequency resistive heaters will certainly continue to be used to improve heavy oil production. Downhole thermocouple or resistance thermometers might be replaced with surface control systems in which the temperature can be inferred without additional connections to the reservoir, thus, simplifying the installation of the heaters.

Very few low-frequency heating systems (distributed or concentrated) are purchased on the basis of regular reservoir/well requirements, as they still considered as experimental. The heater power and the size of the corresponding power supplies are generally overestimated, resulting in higher costs.

Very little use has been made of concentrated inductive heaters. Those used were developed from resistive heating system designs and operated at low frequency.[88] Future designs and field evaluations should establish if the efficiency and useful lifetime of these heaters is better than those of resistive heaters.

High-frequency (300 MHz to 300 GHz) microwave heating has not been extensively field tested. It may be a very good option for the heating of the metallic portions of a well because the circular production tubing can be used as a waveguide with losses. Thus, part of the heat, generated in the metallic walls, is transferred to the surroundings by conduction and convection. The waveguide (or coaxial cable) connections to the reservoir can be excited at different frequencies to obtain different heating profiles in the well walls and in the reservoir.

The nature of the additional high-frequency wave attenuation, because of the threaded production tubing connections, should be measured experimentally. In principle, these disruptions should not be significant because their dimensions are much smaller than that of the wave-

length of the propagating waves. Coiled-tubing microwave transmission should also be evaluated experimentally, in view of the possible wave reflections caused by the changes in the inner diameter of the tubing.

Electrical power losses in steel pipes used in the petroleum industry, either due to low frequency conduction currents, to induced Eddy currents and other losses in the pipes,[89] or to high-frequency radiation transmitted through the pipe used as a waveguide, can be helpful in improving the oil flow in the pipe and avoiding deposits.

The optimal termination of a high-frequency transmission system to the reservoir material so as to achieve maximum power transfer is still a complex problem of antenna design in dissipative media.[90–92]

Finally, if electrical heating systems are used, the existence of electrical connections from the surface to the reservoir could be exploited fully in the development of downhole instrumentation systems.

Nomenclature

a = radius of circular waveguide
A = surface
A_+, A_- = integration constants
A_1, A_2 = constants for liquid hydrocarbon
$\vec{B}$ = magnetic density vector
c = compressibility
C_p = specific heat at constant pressure
C_r = electrical capacitance along the r axis
C_z = electrical capacitance along the z axis
CT = thermal capacitance
CV = fluid capacitance
$\vec{D}$ = electric density vector
$\vec{E}$ = electric field vector
EG = power (energy) gain
f = frequency, Hz
$\vec{H}$ = magnetic field vector
$H_0^{(2)}, H_0^{(2)}$ = Hankel functions
$\vec{i}$ = unit vector
I = electrical current, amperes
Icr = thermal convection current in the r direction
Icz = thermal convection current in the z direction
IVexc = excitation current for the fluid model
ITexc = excitation current for the thermal model
j = imaginary numbers unit
J_0, J_1 = Bessel functions of complex arguments
$\vec{J}$ = vector current density
k = permeability, darcy
K_T = thermal conductivity
L = distance
P = space and time-dependent pressure, Pa
P_{PUV} = electrical power per unit volume, watts/m^3
P_{PUA} = electrical power per unit area, watts/m^2
$p_{n,m}^{TM}$ = constants due to waveguide TM boundary conditions

$p_{n,m}^{TE}$ = constants due to waveguide TE boundary conditions
PE = applied electrical power, kW
$Q(t)$ = time-dependent oil production
$\overrightarrow{Q_T}$ = heat energy flow per unit area and per unit time
$\overrightarrow{Q}_m$ = mass fluid flow per unit area and per unit time
r, φ, z = cylindrical coordinates
r_a, r_b = inner and outer coaxial radii
R_{well} = well pipe radius
$\overrightarrow{S}$ = complex Poynting vector
t = time
T = absolute temperature, Kelvin
TE = waveguide transverse electric mode
TM = waveguide transverse magnetic mode
$\overrightarrow{V}$ = fluid velocity
V = volume
V_r = component of fluid velocity along the r axis
V_z = component of fluid velocity along the z axis
V_0 = wave velocity in free space, $3.0 \times 10^{+8}$ m/s
x, y, z = Cartesian coordinates
Yr = electrical conductance along the r axis
Yz = electrical conductance along the z axis
YTr = thermal conductance along the r axis
YTz = thermal conductance along the z axis
YVr = fluid conductance along the r axis
YVz = fluid conductance along the z axis
Z = wave impedance
Z_0 = free space wave impedance, 377 ohm
α = attenuation constant
α_D = coaxial cable attenuation due to dielectric losses
α_m = coaxial cable attenuation due to wall metallic losses
$\alpha_{n,m}^{TE}$ = waveguide attenuation due to wall metallic losses for TE modes
$\alpha_{n,m}^{TM}$ = waveguide attenuation due to wall metallic losses for TM modes
β = real propagation constant
$\beta_{n,m}^{TM}$ = waveguide TM propagation constant
$\beta_{n,m}^{TE}$ = waveguide TE propagation constant
γ = propagation constant
γ_0 = propagation constant for free space
γ^{coax} = propagation constant for coaxial cable
δ_S = skin depth
ΔQ = increase in oil production, SBLD
ε = permittivity
ε_0 = free space permittivity, $8{,}854 \times 10^{-10}$ farad/m
ε' = real part of the permittivity
ε'' = imaginary part of the permittivity
η = process efficiency

κ_T = thermal diffusivity
$\lambda_{CO,TE11}$ = cutoff wavelength for waveguide TE11 mode
μ = viscosity
μ' = real part of the magnetic permeability
μ'' = imaginary part of the magnetic permeability
μ_M = magnetic permeability
μ_0 = free space magnetic permeability, $4\pi \times 10^{-7}$ henry/m
$\mu(T)$ = temperature-dependent viscosity
ρ = density of hydrocarbon
ρ_c = electrical charge per unit volume
σ = conductivity
σ' = real part of the conductivity
σ'' = imaginary part of the conductivity
σ_M = metal conductivity
σ_{mw} = metal wall conductivity
ν = kinematic viscosity
ϕ = porosity
Φ = potential, volts
ω = angular frequency, radians/s
ω_C^{TM} = cutoff frequency for TM modes
ω_C^{TE} = cutoff frequency for TE modes

Subscripts

a = inner radius
b = outer radius
r, φ, z = cylindrical coordinates
x, y, z = Cartesian coordinates

Acknowledgments

I want to thank my electrical engineering teachers, mainly W.C. Duesterhoeft (Dusty) and Bill Hartwig (U. Texas at Austin), and Lan Jen Chu and Paul Gray (MIT), who showed me how to learn, appreciate, and put my engineering training into practice. I also want to acknowledge the many discussions with Alfredo Essis (formerly with Lagoven PDVSA), Roberto Rodríguez and Ely Schwartz (formerly with PDVSA-INTEVEP), and Humberto Mendoza (PDVSA Exploration and Production), which increased my knowledge of petroleum engineering and oilfield practices.

References

1. Salager, J.L., Briceño, M.I., and Bracho, C.L.: "Heavy Hydrocarbons Emulsions," *Encyclopedic Handbook of Emulsion Technology*, J. Sjöblom (ed.) Dekker, New York City (2001) 455–495.
2. Smalley, C.: "Heavy Oil and Viscous Oil," *Modern Petroleum Technology,* Volume 1 *Upstream,* sixth edition, R.A. Dawe (ed.) Wiley & Sons Inc., New York City (2000) Chap. 11, 409–435.
3. Layrisse, I.: "Heavy Oil Production in Venezuela: Historical Recap and Scenarios for the Next Century," paper SPE 53464 presented at the 1999 SPE Symposium on Oilfield Chemistry, Houston, 16–19 February.
4. Burger, J., Souriau, P., and Combarnous, M.: *Thermal Methods of Oil Recovery,* Technip Editions, Paris (1985) 37–41.

5. Orfeil, M.: *Electric Process Heating,* Bordan Dunod, Paris (1987) 391–621.
6. Davies, E.J.: *Conduction and Induction Heating,* Peter Peregrinus Ltd., London (1990) 93–102.
7. Metaxas, A.C. and Meredith, R.J.: *Industrial Microwave Heating*, Peter Peregrinus Ltd., London (1990) 1–102.
8. Okress, E.C. (ed.): *Microwave Power Engineering,* Volumes 1 and 2, Academic Press, New York City (1968) 1–27.
9. "Historical Perspectives of Microwave Technology," IEEE *Transactions on Microwave Theory and Techniques,* Saad, T.S. (ed.), IEEE Press, New York City, MTT-32, **9** (1984) 955–1271.
10. Farouq Ali, S.M.: "Well Stimulation by Downhole Thermal Methods," *Pet. Eng.* **35,** No. 11, 26.
11. Farouq Ali, S.M.: *Oil Recovery by Steam Injection*, Producers Publishing Co. Inc., Bradford, Pennsylvania (1970) 113–116.
12. Howell, J.K. and Hogwood, E.E.: *Electrified Oil Production,* second edition, PennWell Publishing Co., Tulsa (1981) 235–236.
13. *The Electric Heaters Handbook,* Omega®, Stamford, Connecticut (1995) Z-61.
14. *Electric Heating Products, Controls, and Systems Catalog,* Chomalox®, Pittsburgh, Pennsylvania (1995) A-32.
15. Abernethy, E.R.: "Production Increase of Heavy Oils by Electromagnetic Heating," *J. Cdn. Pet. Tech.* (1976) **15**, No. 3, 91.
16. Gill, W.: "The Electrothermic System for Enhanced Oil Recovery," *First Intl. Conference on the Future of Heavy Crude and Tar Sands,* McGraw-Hill Book Co. Inc., New York City (1979) Chap. 52, 469–473.
17. Vinsome, K. *et al.:* "Electrical Heating," *J. Cdn. Pet. Tech.* (1994) **33,** No. 4, 29.
18. Bridges, J. *et al.:* "Radio Frequency Heating to Recover Oil from Utah Tar Sands," *First Intl. Conference on the Future of Heavy Crude and Tar Sands,* McGraw-Hill Book Co. Inc. (1979) Chap. 44, 396–409.
19. Carlson, R.D., Blasé, E.F., and McClendon, T.R.: "Development of the IIT Research Institute RF Heating Process for In-Situ Oil Shale/Tar Sands Fuel Extraction—An Overview," *Proc.,* 14th Oil Shale Symposium, Golden, Colorado (1981) 138–145.
20. Sresty, G.C., Snow, R.H., and Bridges, J.E.: "The IITRI RF Process to Recover Bitumen from Tar Sand Deposits—A Progress Report," *Proc.,* Second UNITAR Intl. Conference on Heavy Crude and Tar Sands, Caracas (1982) 7–17.
21. Lervik, J.K, Kulbotten, H, and Klevjer, G.: "Prevention of Hydrate Formation in Pipelines by Electrical Methods," Proc. of the 1997 7th International Offshore and Polar Engineering Conference, Part 2 (of 4), Honolulu, Hawaii, 23–30 May.
22. Cheng, Y.M., Guo, C.Z., and Gong, L.: "A Mathematical Model of Electrical Heating in Hollow Pump Rod and Its Application," paper SPE 30317 presented at the 1995 SPE International Heavy Oil Symposium, Calgary, 19–21 June.
23. McGee, B.C.W. and Vermeulen, F.E.: "Electrical Heating with Horizontal Wells, The Heat Transfer Problem," paper SPE 37117 presented at the 1996 SPE International Conference on Horizontal Well Technology, Calgary, 18–20 November.
24. Schild, A.: "A Theory for the Effect of Heating Oil-Producing Wells," *Trans.,* ASME (1957) **210,** 1–10.
25. Todd, J.C. and Howell, E.P.: "Numerical Simulation of In-Situ Electrical Heating to Increase Oil Mobility," *J. Cdn. Pet. Tech.* (1978) **17,** No. 2, 31.
26. Newbold, F.R. and Perkins, T.K.: "Wellbore Transmission of Electrical Power," *J. Cdn. Pet. Tech.* (1978) **17,** No. 3, 39.
27. Harvey, A.H. and Arnold, M.D.: "Selective Electric Reservoir Heating," *J. Cdn. Pet. Tech.* (1978) **17**, No. 3, 47.
28. Harvey, A.H. and Arnold, M.D.: "A Radial Model for Estimating Heat Distribution in Selective Electric Reservoir Heating," *J. Cdn. Pet. Tech.* **19,** No. 4, 37.
29. Vermeulen, F.E. and Chute, F.S.: "Electromagnetic Techniques in the In-Situ Recovery of Heavy Oils," *J. Microwave Power* (1983) **18,** No. 1, 15.
30. McPherson, R.G., Chute, F.S., and Vermeulen, F.E.: "Recovery of Athabasca Bitumen with the Electromagnetic Flood (EMF) Process," *J. Cdn. Pet. Tech.* (1980) **19,** No. 1, 44.

31. Bridges, J.E., Sresty, G.C., and Dev, H.: "In-Situ RF Heating for Oil Sands and Heavy Oil Deposits," paper presented at the 1985 UNITAR/UNDP Intl. Conference on Heavy Crudes and Tar Sands, Calgary, 22–31 July.
32. Bridges, J.E. *et al.:* "Electromagnetic Stimulation of Heavy Oil Wells," paper presented at the 1985 UNITAR/UNDP Intl. Conference on Heavy Crudes and Tar Sands, Calgary, 22–31 July.
33. Killough, J.E. and Gonzalez, J.A.: "A Fully Implicit Model for Electrically Enhanced Oil Recovery," paper SPE 15605 presented at the 1986 SPE Annual Technical Conference and Exhibition, New Orleans, 5–8 October.
34. El-Feky, S.A.: "Theoretical and Experimental Investigations of Oil Recovery by the Electro Thermal Technique," PhD dissertation, U. of Missouri, Rolla, Missouri (1977).
35. Hiebert, A.D. *et al.:* "Numerical Simulation Results for the Electrical Heating of Athabasca Oil Sand Formations," *SPERE* (February 1986) 76.
36. Casey, J.P. and Bansal, R.: "Insulated Dipole Antennas for Heating Oil Shale," *J. Appl. Phys.* (1987) **61,** No. 12, 5455.
37. Callarotti, R.C.: "Reservoir Simulation for the Calculation of Absorbed Electrical Energy in EOR Processes with RF Techniques," *Proc.,* Third Intl. Symposium on Enhanced Oil Recovery, Maracaibo (1989) 1–18.
38. Pizarro, J.O.S. and Trevisan, O.V.: "Electrical Heating of Oil Reservoirs: Numerical Simulation and Field Test Results," *JPT* (October 1990) 1320.
39. Fanchi, J.R.: "Feasibility of Reservoir Heating by Electromagnetic Irradiation," paper SPE 20483 presented at the 1990 SPE Annual Technical Conference and Exhibition, New Orleans, 23–26 September.
40. Baylor, B.A., Maggard, J.B., and Wattenbarger, R.A.: "Improved Calculation of Oil Production Response to Electrical Resistance Heating," paper SPE 20482 presented at the 1990 SPE Annual Technical Conference and Exhibition, New Orleans, 23–26 September.
41. Islam, M.R., Wadarar, S.S., and Bansal, A.: "EOR of Ugnu Tar Sands of Alaska Using Electromagnetic Heating with Horizontal Wells," paper SPE 22177 presented at the 1991 International Artic Technology Conference, Anchorage, 29–31 May.
42. McGee, B.C.W., Sigmund, P. and Spencer, H.L.: "Visco-Skin Effect in Heavy Oil Reservoirs," *Proc.,* Fifth UNITAR/UNDP Conference on Heavy Crudes and Tar Sands (1991) Caracas, **2,** 157–165.
43. Maggard, J.B. and Wattenbarger, R.A.: "Factors Affecting the Efficiency of Electrical Resistance Heating Patterns," *Proc.,* Fifth UNITAR/UNDP Conference on Heavy Crudes and Tar Sands (1991) Caracas, **3,** 519–530.
44. Laine R.E. *et al.:* "Simplified Heavy-Oil Bottomhole Heating Production Predictions," *Proc.,* Fifth UNITAR/UNDP Conference on Heavy Crudes and Tar Sands (1991) Caracas, **3,** 531–537.
45. Marsden, S.S.: "Microwave Heating of Heavy Oil Reservoirs as a Viable Method of EOR," *Proc.,* Fifth UNITAR/UNDP Conference on Heavy Crudes and Tar Sands (1991) Caracas, **3,** 515–518.
46. Callarotti, R.C.: "Circuit Modeling for the Numerical Calculation of RF Heating of Crude Oil in Pipes and Reservoirs," *Proc.,* Fifth UNITAR/UNDP Conference on Heavy Crudes and Tar Sands (1991) Caracas, **3,** 547–559.
47. Callarotti, R.C. and DiLorenzo, M.: "Resistive-Capacitive Tomography," paper 23679 presented at the 1992 SPE Latin American Petroleum Engineering Conference, Caracas, 8–11 March.
48. Sumbar, E., Chute, S., and Vermeulen, F.: "Electromagnetic In-Situ Heating of Heavy Oil Reservoirs to Increase Production Rates," *J. Microwave Power & Electromagnetic Energy* (1992) **27,** No. 2, 67.
49. Dolande, J. and Datta, A.: "Temperature Profiles in Microwave Heating of Solids: A Systematic Study," *J. Microwave Power & Electromagnetic Energy* (1993) **28,** No. 2, 58.
50. Callarotti, R.C.: "Circuital Modeling Applied to Transient Flow Problems in Porous Media," *Proc.,* Third Caribbean Congress on Fluid Dynamics and Latin American Symposium on Fluid Mechanics (1995) Caracas, **2,** C1–C9.
51. Callarotti, R.C.: "Proper Eigenvalue Solution for the Transient Response of Multidimensional Heat Transfer Systems," *Communications in Numerical Methods in Eng.* (1995) **11,** No. 1, 715.

52. Callarotti, R.C. and Mendoza, H.: "A New Approach to the Analysis of the Electrical Heating of Wells and Reservoirs: Circuital Modeling and Efficient Numerical Solutions," paper SPE 36889 presented at the 1996 SPE European Petroleum Conference, Milan, 22–24 October.
53. Soliman, M.Y.: "Approximate Solutions for the Flow of Oil Heated Using Microwaves," *J. Pet. Science & Eng.* (1997) **18,** No. 1, 93.
54. Hu, Y., Jha, K.N., and Chakma, A.: "Heavy-Oil Recovery from Thin Pay Zones by Electromagnetic Heating," *Energy Sources* (1999) **21,** No. 1, 63.
55. Kendall, E.J.M.: "Electrical Conductivity of Medium Heavy Crude Oil," *J. Cdn. Pet. Tech.* (1978) **17,** No. 3, 37.
56. Bridges, J.E., Taflove, A., and Snow, R.H.: "Net Energy Recoveries for the In-Situ Dielectric Heating of Oil Shale," *Proc.,* 11th Oil Shale Symposium, Golden, Colorado (1978) 311–330.
57. Snow, R.H.: "Comparison of Dielectric Heating and Pyrolysis of Eastern and Western Oil Shales," *Proc.,* 12th Oil Shale Symposium, Golden, Colorado (1979) 283–298.
58. Butts, J.R., Lewis, J.E., and Steward, F.R.: "Microwave Heating of New Brunswick Oil Shale," *J. Microwave Power* (1983) **18,** No. 1, 37.
59. Briggs, W.E., Lewis, J.E., and Tranquilla, J.M.: "Dielectric Properties of New Brunswick Oil Shale," *J. Microwave Power* (1983) **18,** No. 1, 75.
60. Sen, P.N. and Chew, W.C.: "The Frequency Dependent Dielectric and Conductivity Response of Sedimentary Rocks," *J. Microwave Power* (1983) **18,** No. 1, 97.
61. Poley, J.P., Nooteboom, J.J., and De Waal, P.J.: "Use of VHF Dielectric Measurements for Borehole Formation Analysis," *The Log Analyst* (1978) **19,** No. 3, 8.
62. Prats, M.: "Procesos Térmicos de Extracción de Petróleo," Ediciones Técnicas Intevep, Los Teques (1987) 118–129.
63. Vermeulen, F.E. and Chute, F.S.: "On the Classification of Processes Using Electric and Magnetic Field to Heat Materials," *J. Microwave Power & Electromagnetic Energy* (1987) **22,** No. 4, 187.
64. Chute, F.S. and Vermeulen, F.E.: "Present and Potential Applications of Electromagnetic Heating in the In-Situ Recovery of Oil," AOSTRA *J. Research* **4,** No. 1, 19.
65. Duncan, G.: "Enhanced Recovery Engineering," *World Oil* (March 1996) 86.
66. Selyakov, V.I. and Kadet, V.V.: *Percolation Models for Transport in Porous Media,* Kluwer Academic Publishers, Dordrecht, The Netherlands (1996) 167–197.
67. *Microwave Aquametry: Electromagnetic Interaction with Water-Containing Materials,* A. Kraszewski (ed.) IEEE Press, New York City (1996) 1–34.
68. *Microwave Enhanced Chemistry,* H.M. Kingston and S.J. Haswell (eds.), American Chemical Society, New York City (1997) 3–53.
69. Adler, R.B., Chu, L.J., and Fano, R.M.: *Electromagnetic Energy Transmission and Radiation,* Wiley & Sons Inc., New York City (1960) 22–24.
70. Ramo, S., Whinnery, J.R., and Van Duzer, T.: *Field and Waves in Communication Electronics,* Wiley & Sons Inc., New York City (1965) 322–370.
71. Stratton, J.: *Electromagnetic Theory,* McGraw-Hill Book Co. Inc., New York City (1941) 349–362.
72. Moon, P. and Spencer, D.E.: *Field Theory for Engineers,* Van Nostrand, Princeton, New Jersey (1960) 469–471.
73. Moon, P. and Spencer, D.E.: *Foundations of Electrodynamics,* Boston Technical Publishers Inc., Cambridge (1965) 174.
74. *Handbook of Mathematical Functions,* M. Abramowitz and I.A. Segun (eds.), Dover Publications, Inc., New York City (1965) 358–364.
75. Collin, R.E.: *Foundations for Microwave Engineering,* McGraw-Hill Books Kogakusha, Tokyo (1966) 109–111.
76. Callarotti, R.C. and Alfonzo, M.: "Measurement of the Conductivity of Metallic Cylinders by Means of an Inductive Measurement," *J. Appl. Phys.* (1972) **43,** No. 7, 3040.
77. Callarotti, R.C., Schmidt, P., and Arqué, H.: "Theory of the Measurement of Thickness and Conductivity of Cylindrical Shells by Means of an Inductive Method," *J. Appl. Phys.* (1972) **43,** No. 10, 3952.
78. Golan, M. and Whitson, C.H.: *Well Performance,* IHRDC Publishers, Boston, Massachusetts (1986) 442.